Earth-Science Reviews 224 (2022) 103876

Contents lists available at ScienceDirect

Earth-Science Reviews

journal homepage: www.elsevier.com/locate/earscirev

Seismic facies analysis: Past, present and future

Guoqiang Xu [a,b,*], Bilal U. Haq [c]

[a] State Key Laboratory of Oil and Gas Reservoir Geology and Exploitation, Chengdu University of Technology, Sichuan 610059, China
[b] College of Energy Resources, Chengdu University of Technology, Sichuan 610059, China
[c] Sorbonne University, Institute of Earth Sciences, Paris, France and Smithsonian Institution, Washington, DC, USA

ARTICLE INFO

Keywords:
Seismic facies analysis
Seismic lithofacies analysis
Seismic geomorphology
Seismic sedimentology
Artificial intelligence
South China Sea

ABSTRACT

Seismic facies and lithofacies analysis, once considered a breakthrough in exploration applications, is currently a dynamic field because of the addition of several new concepts and interpretive procedures. In terms of basic theory, notable developments have taken place that encompass refinements in geological and geophysical concepts, including several enhancements to sequence-stratigraphic and facies distribution models, better knowledge of seismic response mechanism to small-scale stratigraphic structures and different rock types, as well as the emergence of new technologies, such as the one allows the restoration of original depositional architecture and spectral decomposition. A seismic facies analysis index system is proposed that includes nine independent parameters: position, external form, internal configuration, continuity, smoothness, amplitude, frequency, special waveforms, and appearance. The sedimentary systems established by traditional seismic facies analysis lack detailed lithofacies and hydrodynamic information. However, presently further subdivision of seismic lithofacies into more detailed categories is now possible, made available by the addition of new seismic parameters that are indicative of sedimentary structure and rock-type combinations. This enables interpreters to identify lithofacies details directly from the seismic data and reconstruct the sedimentary systems with greater precision (by superposition of the environment, lithofacies and flow paths). The seismic slice image analysis, including seismic geomorphology and seismic sedimentology, employs a stratal time slice, 90° phase shift, and spectral decomposition techniques to improve the resolution of the slice images, describe sedimentary micro-facies and understand sedimentary processes based on the geometric features of the time slice. The seismic facies auto-classification techniques are still at an early stage of development, but significant possibilities exist for future enhancements if the new seismic index system, where the accumulated knowledge of the skilled experts could be utilized advantageously. This paper will also serve as a summary of the state-of-the-art of seismic facies analysis.

1. Introduction

With the development of rapid digital computing in the 1970s, wavelet side lobes of seismic data could be suppressed by zero-phase processing (Widess, 1973) leading to the correlation of sharp seismic reflections with bedding and other physical boundaries that in turn led to the use of seismic data for investigating subsurface stratigraphic configurations and sedimentary facies (Sangree and Widmier, 1977; Mitchum et al., 1977a, 1977b; Anstey, 1980). This in turn facilitated the advent of seismic stratigraphy (e.g., Vail et al., 1977) that was considered a technological revolution in exploration geology. Seismic stratigraphy involves subsurface geologic interpretations using seismic data that integrates geophysics and geology (Mitchum et al., 1977a, 1977b; Badley, 1985; Sheriff, 1985). One useful aspect of the discipline was seismic facies analysis (Berg, 1982) accomplished by examining reflection geometries and stratal architecture and grouping them as depositional sequences to interpret the paleoenvironment and infer seismic lithofacies (Mitchum et al., 1977a, 1977b; Roksandic, 1978).

At the early stage of this research seismic facies analysis was developed by geologists and geophysicists working together to ensure that both the kinematic and dynamic aspects of seismic imaging and geologic features of interest could be captured and the geological implications of seismic information could be inferred scientifically (Xu et al., 1990; Chopra and Marfurt, 2012) (Fig. 1). The emergence of sequence stratigraphy has attracted a large number of geologists to participate in the geological research related to seismic facies analysis, but reduced the depth of cooperation between geophysicists and geologists. Geologists independently engaged in sedimentological and stratigraphic studies of

* Corresponding author at: State Key Laboratory of Oil and Gas Reservoir Geology and Exploitation (Chengdu University of Technology), Sichuan 610059, China.
E-mail address: xuguoqiang@mail.cdut.edu.cn (G. Xu).

https://doi.org/10.1016/j.earscirev.2021.103876
Received 24 August 2021; Received in revised form 21 November 2021; Accepted 25 November 2021
Available online 29 November 2021

the outcrop, well, and seismic data, while the geophysicists started employing seismic attributes, such as amplitude and frequency, to characterize reservoir properties in hydrocarbon exploration (Wang and Shi, 1998).

Over the last three decades, based on different seismic and sequence-stratigraphic models (e.g., Vail et al., 1991; Mitchum and Van Wagoner, 1991; Ravenne, 2002; Catuneanu et al., 2009; Zhu, 2018; Catuneanu, 2019; Xu et al., 2020; Xu and Pang, 2021), geologists have proposed several models that translate seismic facies into sedimentary facies (e.g., Berg, 1982; Klein, 1985; Mutti and Normark, 1991; Galloway and Hobday, 1996; Nilsen et al., 2007; Batchelor et al., 2013; Matenco and Haq, 2020). Furthermore, by identifying new parameters (Kirk, 2016; Xu et al., 2021), geologists have improved their ability to differentiate additional geological features and classify seismic lithofacies in greater detail. Simultaneously, geophysicists have developed several techniques to improve seismic resolution (e.g., Partyka et al., 1999; Vermeer, 1998; Zeng et al., 1998; Miall, 2016), information visualization (Brown, 2011), and auto-classification of seismic facies (e.g., Love and Simaan, 1984; Barnes, 1994; Meldahl et al., 2001; West et al., 2002; Coleou et al., 2003; Chopra and Marfurt, 2012). These techniques include seismic geomorphology (e.g., Brown et al., 1982; Posamentier, 2000, 2001; Posamentier and Kolla, 2003; Posamentier et al., 2007), seismic sedimentology (e.g., Zeng et al., 1998; Hubbard et al., 2011; Zeng, 2013; Zeng, 2018), waveform classification (e.g., Addy, 1998; Salganicoff et al., 1988; Song et al., 2017) and multi-attribute classification (e.g., Barnes, 1994; Ao et al., 2019), among others. Based on these developments three new working schemes have been proposed (Fig. 1), i.e., enhanced seismic lithofacies analysis, seismic time-slice image analysis and auto-classification of seismic facies.

In this paper the concepts and principles of seismic facies analysis are reviewed from the perspective of geologists, and we make an attempt to discuss the implications of combining geology and geophysics of seismic data interpretation through the relationships (or "dialogue") between the lithological section and the seismic records. The progress in these three aspects of the basic knowledge of the combination of seismics and geology, the parameters of seismic facies analysis and the stratagem of this analytical technique in the past 40 years are systematically summarized. The future prospects of seismic facies analysis are discussed in the last part of the paper.

2. Fundamentals of seismic geological interpretations

Since the early 1970s, when seismic data gathering and processing entered the digital age, seismic technology has developed rapidly. Modern seismic data contain an extraordinarily rich amount of information that includes many new precepts and terms, and now almost all interpretations of seismic data are accomplished through observations and manipulations on workstations. Currently, by observing the stratal configurations afforded by seismic reflections patterns, interpreters can obtain lithological and hydrocarbon-related information offered by seismic attributes, such as amplitude, frequency, and waveforms (e.g., Meckel and Nath, 1977; Anstey, 1980; Weidess, 1982; Badley, 1985; Xu et al., 1990; Liu, 1997; Brown, 2011; Wang et al., 2015; Xu and Pang, 2021). Accordingly, to work effectively with seismic data various basic features need to be mastered that include minimum-phase and zero-phase wavelets, positive and negative reflections, polarity display, phase shifting, amplitude tuning, readable and discernible thickness, resolution limitations, types of basic waveforms (Anstey, 1980), Boit-Geerstma equation and the Dominico effect (Domenico, 1977), cumulative thickness effect of thin interlayers, Fresnel zone, bright spots, American and European polarities, and spectral decomposition (Brown, 2011). Additionally, appropriate skills are needed for techniques involving synthetic seismograms, seismic modeling and seismic slicing, among others (Wang et al., 2015; Guo et al., 2021; Xu et al., 2021). The following is a summary of the basic knowledge needed for detailed integration of seismic geophysical and geological parameters.

2.1. Zero-phase processing

The field wavelet triggered by blasting, gravity hammering, or the use of air gun is also known as the minimum-phase wavelet (Badley, 1985; Brown, 2011), which is composed of multiple phases, where the energy of the head phase is stronger (Fig. 2a) than the energy from the middle to the tail phases where it weakens gradually. After deconvolving, the minimum-phase wavelet is transformed into a nearly symmetric waveform wavelet composed of one main lobe and two side lobes (Fig. 2b). Following displacing and shaping treatments, the main lobe moves to the position of the geological interface where the corresponding time is zero, the two side lobes become symmetrical (e.g., Sheriff and Margaret, 1980; Simm and White, 2002), while the minimum-phase wavelet becomes a zero-phase wavelet (Ricker, 1953) (Fig. 2d). In seismic profiles that have undergone zero-phase processing, the surface of the seafloor is often represented by a complete zero-phase wavelet reflection (Fig. 2e).

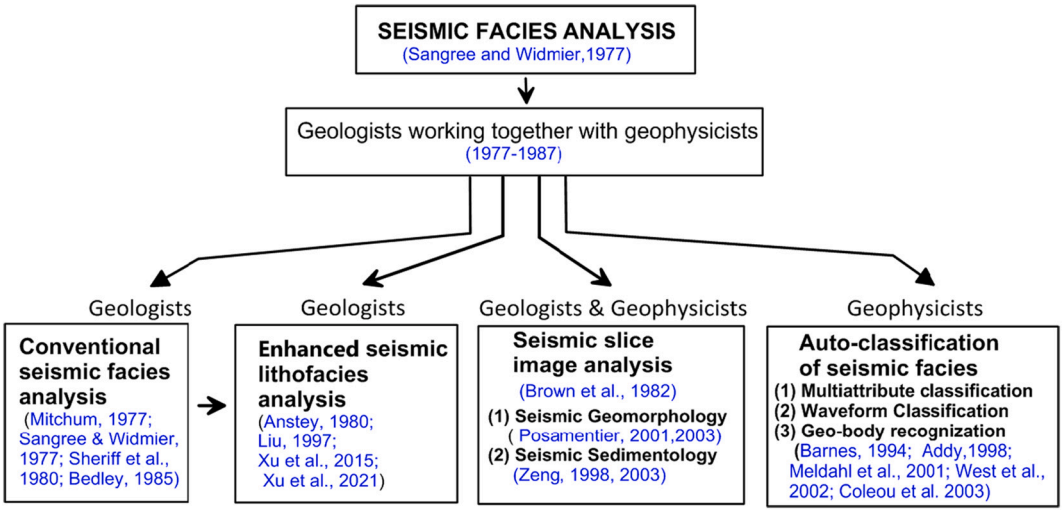

Fig. 1. History of seismic facies analysis and the emergence of three new subdisciplines along side the traditional (conventional) seismic facies analysis of the 1970s and 80s.

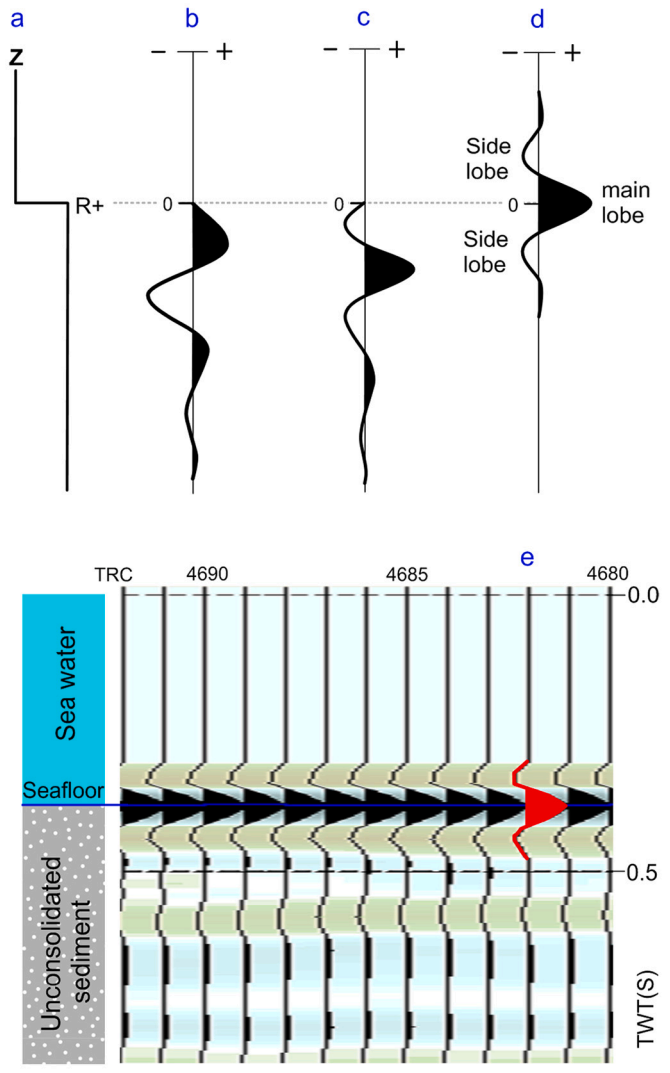

Fig. 2. Diagram showing zero-phase processing (modified form Sheriff and Margaret, 1980). a. An impedance curve. b. The minimum-phase wavelet; c. The first derivative waveform of minimum-phase wavelet; d. Zero-phase wavelet with symmetrical side lobes; e. The reflection of seafloor surface.

2.2. American and European polarities

Over the years, different organizations have defined their own polarity displays. Because polarity is reversed repeatedly in seismic data, the polarity (termed as positive or negative) is often unclear not only to interpreters, but sometimes also to the technicians processing the data (Brown, 2011). Many diagnostic methods have been proposed and American and European polarities have been defined to avoid such confusion (Rankey, 2017). In American polarity, the peak is assigned as the center lobe of the positive reflection (the interface from low impedance to high impedance, Fig. 3), whereas the trough is assigned as the center lobe of the negative reflection (the interface from high impedance to low impedance) (Wang et al., 2015). In contrast, following the Society for Exploration Geophysicists' recommendations for European polarity, the trough of the zero-phase wavelet is used as the center lobe of positive reflection and the peak as the center lobe of negative reflection (Badley, 1985). However, as American polarity is compatible with the pseudo-log display, it has become more popular in the exploration industry (Brown, 2011).

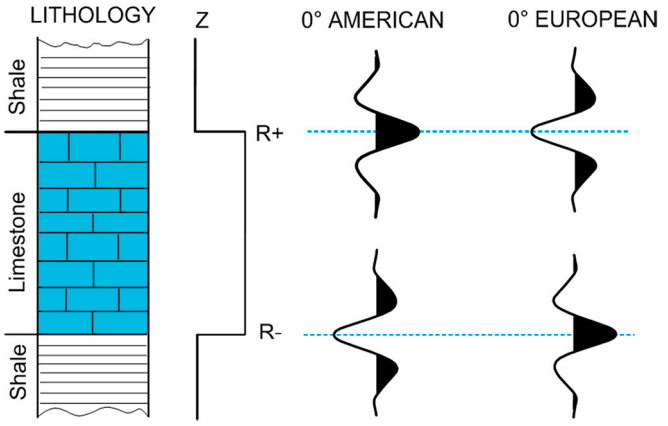

Fig. 3. American and European polarity schemes (modified form Wang et al., 2015). Abbreviations: Z— acoustic impedance; R— reflection coefficient; 0°— zero-phase wavelet.

2.3. The limit of discernibility in seismic data

The resolution of zero-phase data is one-quarter of the dominant wavelength (λ) for an interlayer with opposite polarity at the top and bottom (dipolar interlayer, Fig. 4a) (e.g., Ricker, 1953; Widess, 1973; Anstey, 1977; Anstey, 1980; Brown, 2011). It is λ/4.6 for an interlayer with the same polarity at the top and bottom (homopolar interlayer, Fig. 4b) (Badley, 1985). The limit of discernibility is approximately one-sixtieth (the amplitude of the composite wave is approximately 25% of a single reflection, Figs. 4a) in the most favorable instance for a dipolar interlayer (Brown, 2011), and it is only λ/4.6 for a homopolar interlayer (e.g., Badley, 1985; Wang et al., 2015) (Fig. 4b).

2.4. Readable and detectable thicknesses

When the thickness of the interlayer is greater than a quarter of the wavelength, the seismic top and bottom are consistent with the interlayer top and bottom, and the time thickness can be read directly from the seismic profile (e.g., Neidell and Poggiagliolmi, 1977; Anstey, 1980; Brown, 2011; Wang et al., 2015). When the thickness is less than λ/4, the seismic top is higher than the interlayer top and the seismic bottom is lower than the interlayer bottom, and the period from the seismic top to the seismic bottom is greater than the interlayer thickness (Fig. 4a). In this instance, the interlayer thickness ($h < \lambda/4$) can be detected through the composite wave amplitude as this decreases linearly with the thickness (Anstey, 1980).

2.5. Skew-symmetrical waveform

The low-impedance gas-bearing sandstone and high-impedance limestone encased by shale show skew-symmetrical wave with extra-large amplitude (Figs. 5b and c), which was defined first by Anstey (1980) as, "the skew-symmetry is about an *upward-going zero-crossing* for gas sandstone and about a *downward-going zero-crossing* for limestone. Such a skew-symmetric waveform description (upward-going or downward-going) starts from the crest generated by the positive reflection interface, and "zero crossing" is a point where the amplitude is zero, the dividing line between a trough and a peak. However, this is not easy to use in practice. Skew-symmetrical waves can be found in seismic data in both low-impedance layer (such as porous gas sandstone) and high-impedance layers (such as limestone) encased in shale.

Distinguishing these two waveforms is very important for lithofacies identification and oil and gas exploration. In order to effectively apply this waveform, Xu et al. (2015, 2021) redefined the two skew-symmetric waveforms: a combined wave generated by a low-impedance interlayer known a right-downward skew-symmetrical wave (RD-wave)because of

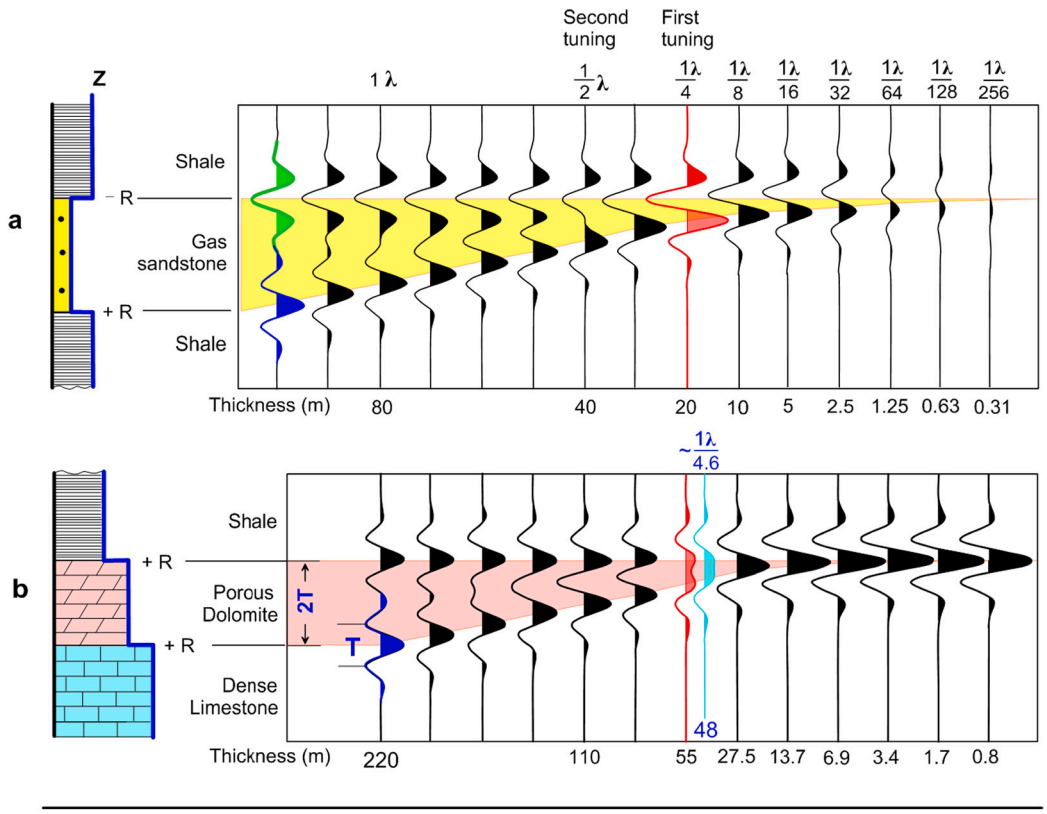

Fig. 4. Horizontal variation in the seismic waveform of a wedge-shaped interlayer. Zero-phase wavelet and American polarity are displayed. a. Seismic response of a wedge-shaped sandstone lodged within shales (compiled from Anstey, 1980; Brown, 2011). If the velocity of porous sandstone at shallow depths is significantly lower than that of the shale, then the sand produces a negative reflection on top and a positive reflection on the bottom; the top and bottom reflections (a symmetrical waveform shown in green and blue colors) can be completely separated when the thickness of sand is greater than 1λ. If the thickness is less than λ/2, the two reflection pulses overlap and interfere to form a skew-symmetrical complex waveform. If the thickness is equal to or greater than λ/4, the amplitude of composite wave reaches the maximum (tuning amplitude), and the time thickness can be directly read from the composite wave. When the thickness is less than λ/4, the period from trough (corresponding to the top interface) to peak (corresponding to the bottom interface) is greater than the interlayer thickness, the shape of the complex reflection does not change, and the thickness is proportional to the amplitude. When the thickness is λ/64, the composite wave is still visible because the amplitude of composite wave is about 22% of a single reflection. b. Seismic response of carbonate weathered crust (compiled from Badley, 1985; Wang et al., 2015). Reflections from top and bottom interfaces are positive, and the limit of separability is λ/4.6. If the thickness is between 0.28λ and 0.18λ, a low-frequency waveform will be generated. When the thickness is less than ~λ/4, the two events corresponding to the top and bottom of the reservoir will disappear. (For interpretation of the references to colour in this figure legend, the reader is referred to the web version of this article.)

the right-downward line (marked with red arrow) from the trough (P2, Fig. 5b) to the peak (P3, Fig. 5b); and the composite wave generated by a high-impedance interlayer is called the left-downward skew-symmetrical wave (LD-wave) (Fig. 5c). These two skew-symmetries can be used to identify large amplitude reflections generated by the high-impedance and low-impedance layers, respectively. Since the low-impedance interlayer of λ/16 to λ/64 has obvious seismic reflection, the RD-wave is particularly useful for recognizing porous sandstone (Anstey, 1980; Wang et al., 2015; Xu et al., 2021) and porous dolomite reservoirs (Fig. 5).

2.6. Ninety-degree phase shift

Seismic wavelets can be transformed into various wavelet phases through phase shifting (Fig. 6a). After phase shifting of 90°, the symmetric waveform becomes the skew-symmetrical waveform (top of Fig. 6a), and the skew-symmetrical waveform becomes symmetric waveform (bottom of Fig. 6a), and they are the first derivatives of each other (Fig. 6b). The 90° phase shifting changes the seismic reflection of the thin sandwich from the two main lobes to one, which allows the thin interlayer to correspond one-to-one to the reflection event. However, it also changes the waveform from the top or bottom interface of the thick layer from one main lobe to two main lobes (top of Fig. 6a and b), which confuses the rule that a stratigraphic interface corresponds to a reflection event. Therefore, the 90° phase data (Fig. 6) is used mainly for thin-layer reservoir study in a 3d block (Brown, 2011; Miall, 2016; Zeng, 2018).

3. Parameters of seismic facies analysis

3.1. Overview

A seismic facies unit can be defined as a sedimentary unit of which the seismic signatures differ from those of the adjacent units (Mitchum et al., 1977a, 1977b). In seismic facies analysis the following parameters should be considered, namely, position (regional setting), external form, internal configuration, reflection amplitude, dominant frequency, reflection continuity, interval velocity, areal association of seismic facies units, abundance of reflections, line direction (dip or strike section), reflection termination, size, formation thickness, slope break, reflection smoothness, special waveform pattern, appearance, reflection polarity, acoustic impedance, bright spots, amplitude variation with offset (AVO) and AVO-derived attributes, arc length and loop area (amplitude-derived attributes), curvature, plane geometry of seismic slice, and the like (e.g., Mitchum et al., 1977a, 1977b; Sangree and Widmier, 1977; Roksandic, 1978; Anstey, 1980; Sheriff and Margaret, 1980; Brown et al., 1982; Badley, 1985; Liu, 1997; Chopra and Marfurt, 2007; Brown, 2011; Miall, 2016; Xie et al., 2017; Verma et al., 2018; Kumar et al., 2019; Xu et al., 2021). There are dozens of seismic signatures and hundreds of derived attributes for seismic facies recognition (Brown, 2011); however, only nine main independent seismic parameters and one geological parameter can be readily used for seismic lithofacies analysis (Fig. 7).

Position, external form, internal configuration, amplitude, frequency and continuity are six independent parameters most commonly used

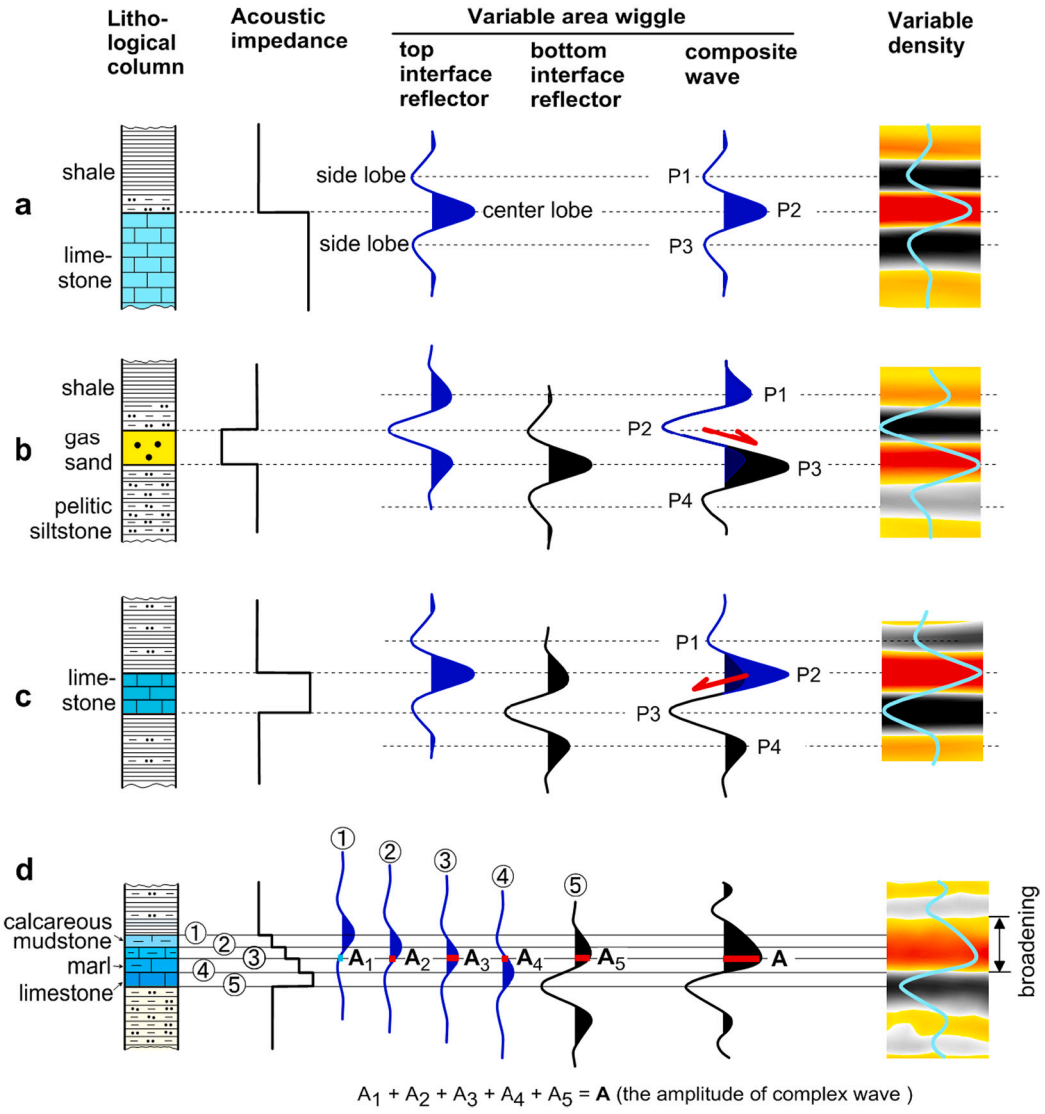

Fig. 5. Three basic seismic waveforms. Zero-phase wavelet and American polarity are displayed. P1 to P4 are lobe numbers (from Xu et al., 2021). a. Zero-phase symmetrical wave generated by a single interface; b. Right downward (red arrow) skew-symmetrical waveform generated by a low-impedance gas sands; c. Left downward (red arrow) skew-symmetrical waveform generated by a high-impedance limestone. d. Diagram showing the composition and decomposition of seismic wave. The amplitude of composite wave at each sampling point is the sum of amplitude of reflections at five interfaces. This type of complex wave is called a low frequency waveform, which is manifested by the broadening of the wave crest (or the reducing of the frequency) corresponding to the transition layer. (For interpretation of the references to colour in this figure legend, the reader is referred to the web version of this article.)

since the emergence of seismic facies analysis (Fig. 7). In addition to this, interval velocity was used widely to interpret lithology in the early years. However, this lost favor in the 1990s because of its low precision (Badley, 1985; Liu, 1997), and was replaced by acoustic impedance inversion and wave pattern analysis (Brown, 2011). Reflection smoothness, waveform (special pattern), and seismic profile appearance are three newly added common elements in seismic lithofacies analysis (Xu et al., 2021). Wave pattern contains two parameters, namely, reflection polarity and acoustic impedance. In terms of their geological and geophysical meaning, the external form and internal configuration of a seismic facies unit and reflection continuity are classified as broader geometric attributes, whereas reflection smoothness and seismic profile appearance are considered as smaller scale geometric attributes. Amplitude, frequency, and wave pattern are dynamic attributes, whereas position and relationship with other units have spatial and geological connotations. Provenance is a very important geological parameter, which is mainly used to determine whether the deep-water fan sand body is sandstone or siltstone. As seismic data cannot distinguish the grain size of siliceous clastic rocks, the sandstone seismic lithofacies obtained by enhanced seismic lithofacies analysis include conglomerate, sandstone, and siltstone. The grain size of deep-water fan sandstone is the same as that of its parent rock, so the grain size can be determined from its parent rock. Therefore, this parameter can only be used after the depositional system has been reconstructed (Xu et al., 2021).

The ten parameters mentioned (i.e. six of the most commonly used parameters in traditional seismic facies analysis and four of the newly added parameters in enhanced seismic lithofacies analysis, Fig. 7) constitute a complete index system for seismic facies analysis. All major sedimentary environments, detailed seismic lithofacies, and some special sedimentary microfacies can be distinguished directly from seismic profiles without necessity for calibration with drilling data (Xu et al., 2021).

3.2. Position, external form and internal configuration and their interrelationships

3.2.1. Position

Position is a spatial indicator for sedimentary facies interpretation and is a parameter for seismic facies analysis, as many sedimentary bodies exist in specific locations (Fig. 8). For example, large reefs are usually found at the edge of platforms or continental shelf margins (Bubb and Hatlelid, 1977), deep-water fans are found on slopes and in deep-sea basins, and a large number of volcanic cones are found in the transitional ocean-continental crust. Based on the interpretation of the regional seismic profile, the position of the seismic facies unit can be

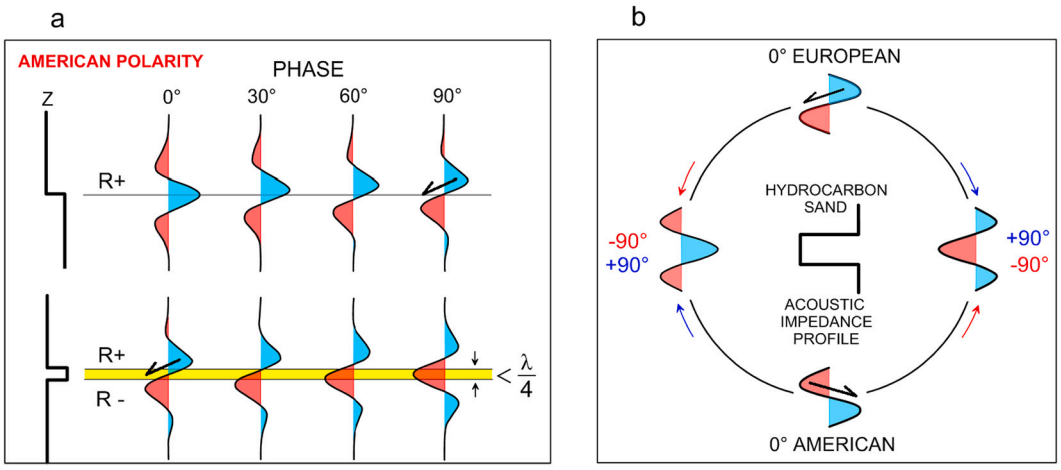

Fig. 6. Diagram showing phase shifting and polarity. a. Seismic waveform after phase shifting (modified form Zeng, 2011): The wave generated by a single positive reflection interface is symmetric, where the center lobe is a peak. A 90° phase wave of this single reflection shows as a "differential" or left downward symmetrical wave. The composite wave generated by a thin compact sandstone shows as a left downward symmetrical wave, in which the center lobe is a trough after the 90° phase shifting. b. Phase shifting and polarity, the arrow colour is consistent with the digital colour (modified from Brown, 2011): A composite wave of thin gas sand may be shown as left downward skew-symmetrical wave (European polarity) or right downward skew-symmetrical wave (American polarity). After a 90°phase shifting (clockwise), they become a zero-phase wave with trough-center-lobe or a zero-phase with peak-center-lobe wave. Conversely, after a − 90° phase shifting (counterclockwise), they become a zero-phase wave with peak-center-lobe wave (European polarity) or a zero-phase wave with trough-center-lobe (American polarity). (For interpretation of the references to colour in this figure legend, the reader is referred to the web version of this article.)

Parameters	Position	External form	Configuration	Continuity	Amplitude	Frequency	Interval velocity	Polarity	Smoothness	Wave pattern	Appearance	Provenance
Mitchum et al., 1977	▲	★	★	★	○	○	○	○				
Roksandic, 1978	▲	★	★	★	○	○	○	○				
Sheriff, 1980	▲	★	★	★	○	○		○	☆			
Bedley, 1985	▲	★	★	★	○	○		○				
Xu et al., 1990	▲	★	★	★	○	○						
Posamentier, 2007	▲	★	★	★	○	○					(Roughness) ☆	
Xu et al., 2021	▲	★	★	★	○	○			☆	○	☆	●

★ Large scale geometric parameter ○ Dynamic attribute ● Geological parameter
☆ Small scale geometric parameter ▲ Spatial location

Fig. 7. Major independent parameters of seismic facies analysis used by various authors.

determined roughly, after which the sedimentary facies can be inferred according to existing sedimentary facies models (e.g., Berg, 1982; Vail et al., 1991; Catuneanu et al., 2009; Matenco and Haq, 2020; Xu and Pang, 2021) and other indicators.

3.2.2. *External form*

In the 1970s and 80s, the external form of a seismic facies unit was observed mainly by means of seismic profiles. External structures can now be observed directly through (time/depth) slices and three-dimensional visualization. The external form of the units can be divided roughly into seven categories, i.e., sheet, wedge, bank, lens, mound, fan, and concave (Mitchum et al., 1977a, 1977b; Sangree and Widmier, 1977). In the modified scheme shown here, three aspects of the previous classification have been modified: (1) Sheet drape is classified as a secondary type of the sheet form; (2) Fan shape is classified as a first-order external form because the fan is hilly only in the strike section, wedge-shaped in the dip section, and fan-shaped in the plane and three-dimensional view; (3) Fill shape has been renamed concave shape because the filling emphasizes sedimentary features, whereas the concave surface emphasizes the external geometry. The concave shape of incised valley is a very important shape of the sedimentary body, which includes river channels, gullies, channels, canyons and troughs, which can be filled or remain unfilled.

3.2.3. *Internal configuration*

Internal configuration refers to the permutation and combination

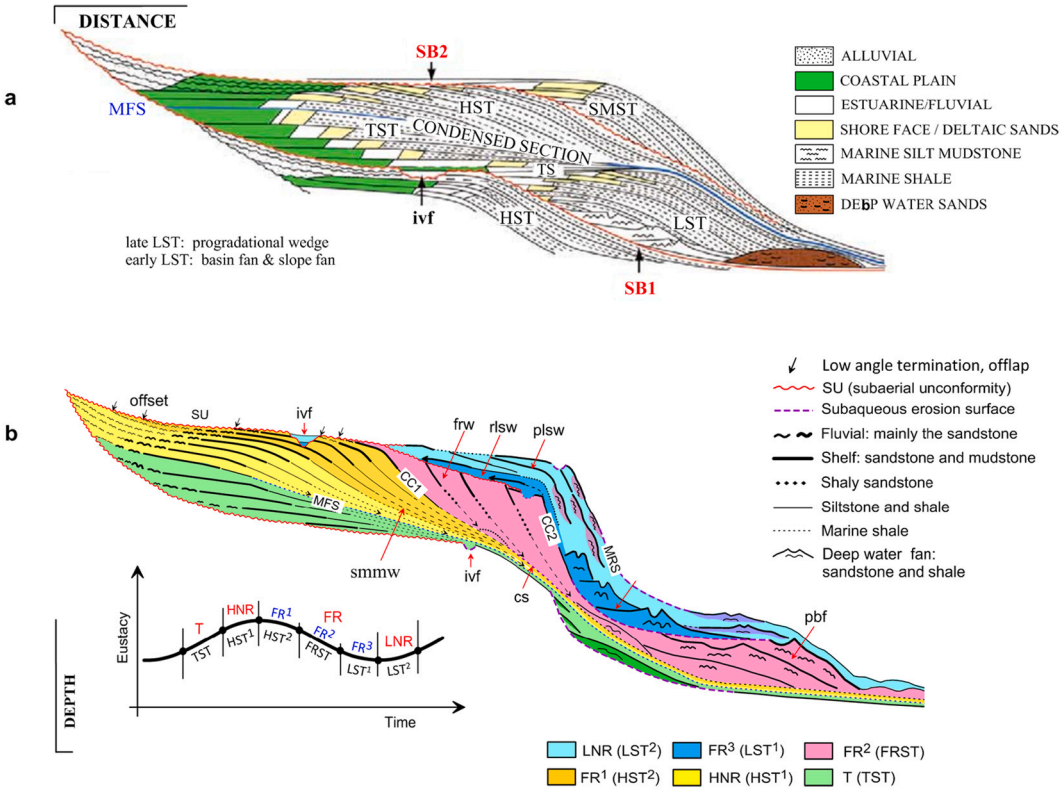

Fig. 8. Sequence stratigraphic architecture and facies distribution. a. The traditional model, modified from Ravenne, 2002; from Vail et al., 1991; b. the modified model, after Xu and Pang, 2021. This new model used the basic sequence stratigraphic framework which is composed of four genetic units (proposed by Catuneanu et al., 2009). Abbreviations: SU – subaerial unconformity; MFS – maximum flooding surface; CC1 – correlative conformity corresponding to the SU of the HNR unit; CC2 – correlative conformity corresponding to the SU of FR unit; MRS – maximum regressive surface. T – transgression; HNR – highstand normal regression; FR – forced regression, including three subunits of FR1, FR2 and FR3; LNR – lowstand normal regression; TST – transgressive systems tract; HST1 – early highstand systems tract; HST2 – late highstand systems tract; FRST – forced regressive systems tract; LST1 – early lowstand systems tract; LST2 – late lowstand systems tract; smmw — shelf margin muddy wedge (this is unique to HST); frw – forced regressive wedge; pbf – prograded basin fan; rlsw – retrograded lowstand wedge; rsf – retrograded slope fan; plsw – prograded lowstand wedge; ivf – incised valley fill; and cs – condensed section; SB1 –type 1 sequence boundary; SB2 –type 2 sequence boundary.

mode of reflection events within a seismic facies unit, which mainly reflect the stratigraphic structure and can be divided roughly into eleven types (Fig. 9), among which the prograding clinoforms include five secondary patterns. Compared with the original classification scheme of Mitchum et al. (1977a, 1977b), the later scholars (e.g., Xu et al., 1990; Posamentier and Kolla, 2003 ; Catuneanu et al., 2009) modified it in four aspects:

(1) Three types of additional internal configurations are added, i.e., stratiform, granular, and convergent. Stratiform is an intermediate configuration between granular and subparallel (Fig. 9). The difference between stratiform and chaotic configurations is that the length, amplitude, and attitude of the reflection events are different in the chaotic configuration, whereas they are roughly the same in the stratiform configuration. Granular is a reflection configuration comprising extremely short events (grainy look), with weak medium amplitude, found in large sets of shallow-water limestones, massive conglomerates, volcanic agglomerates, and volcanic intrusive rock masses (Fig. 10b). Divergent and convergent configurations have been subdivided because they have different geological implications (Fig. 10e). The former emphasizes the basinward *syn*-sedimentary thickening of the strata caused by an increase in the accommodation space, whereas the latter emphasizes the basinward syn-sedimentary thinning of the strata caused by a decrease in the sediment supply.

(2) In the early classification diagrams, the scale of the five oblique configurations was incongruous. Height of clinoforms in parallel and shingled configurations is reduced because they are formed in shallow-water environments (e.g., the middle to outer continental shelf). However, the height of clinoforms in oblique, sigmoid, and complex sigmoid–oblique configurations is increased because they are formed when rivers flow into deep-water environments (e.g., the edge of the continental shelf).

(3) The top surface of the prograding clinoforms is modified from the horizontal plane (Mitchum et al., 1977a, 1977b) to the inclined plane toward the basin (Catuneanu, 2019).

(4) The structure of the wave configuration is modified from a synchronous folded layer to an asynchronous undulating layer (Fig. 9). Wavy reflection often occurs in deep water slope environment (Fig. 11i), which may be related to the plastic flow of mudstone layer. The wave configuration developed on the turbidite levee slope are formed by sedimentation, and Posamentier and Kolla (2003) proposed that this wavy shape may be related to the overflow of the adjacent channel.

3.2.4. The relationship between external geometry and internal configuration

The external form of sedimentary bodies is often correlated with the internal configuration (e.g. Berg, 1982; Pacht et al., 1993; Prather et al., 1998), and the geometry of many depositional bodies has obvious directionality (Fig. 10a). When the relationship among the external form, internal configuration, and spatial setting is known, sedimentary

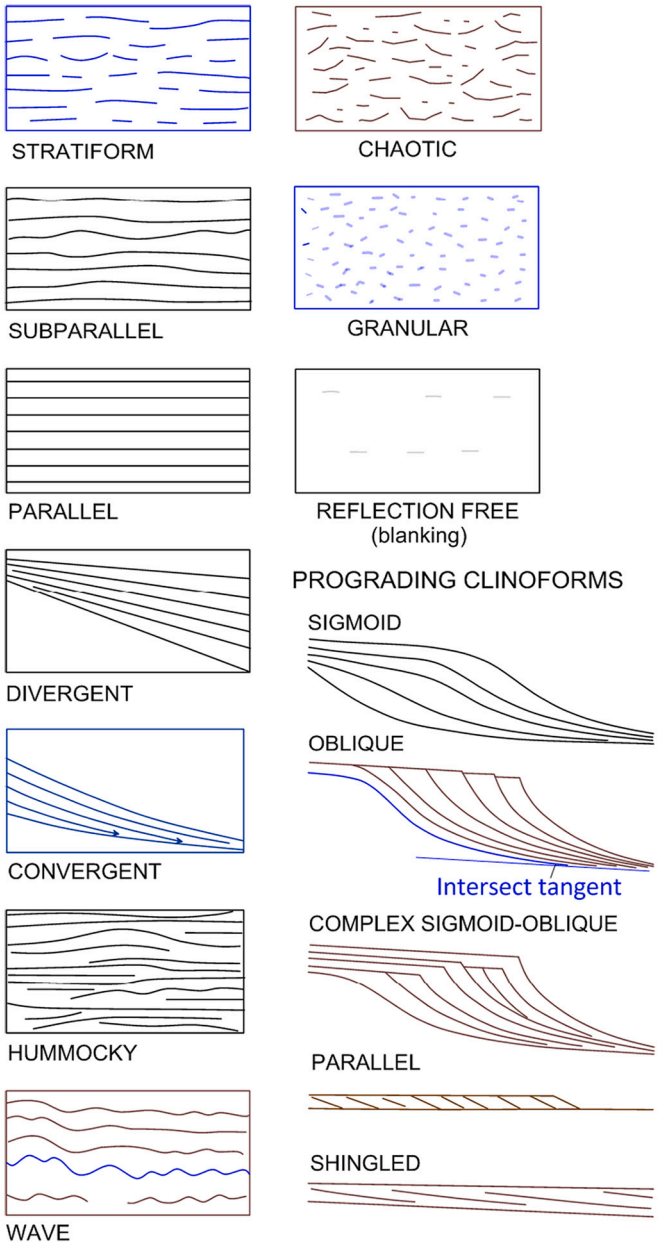

Fig. 9. Independent seismic reflection configurations (modified from Mitchum et al., 1977a, 1977b). The internal configuration diagram shown by the black line is not modified; the brown ones are modified; the blue ones are new additions. (For interpretation of the references to colour in this figure legend, the reader is referred to the web version of this article.)

bodies and the general lithofacies can be diagnosed with -greater confidence.

3.2.4.1. The internal configurations of mounded-shape reflectors. Mounds can be generated by both sedimentary and non-sedimentary bodies (Fig. 10). Dome-shaped sedimentary bodies feature a dome-shaped outline on a strike line and wedge-shaped (with a hummock-shaped) outline in a dip line, and the inner reflection events converge toward the basin (Fig. 10a). Generally, dome-shaped deltaic lobes are formed when rivers flow into deep-water environments (e.g., shelf margins, shelf sags, etc.), where the deltaic plain and delta front subfacies are sand rich, with layered horizontal reflections of low frequency, medium to strong amplitude and moderate continuity; the delta front slope shows a weak amplitude oblique reflection layer, which migrates to the basin continuously; turbidite reflections with low to medium amplitude and medium to high frequency often occur below the delta slope and migrate to the basin together with delta progradation (e.g., Berg, 1982; Posamentier and Allen, 1999; Xu et al., 2006; Gong et al., 2016) (Fig. 10a). However, the shallow-water delta front slope is not obvious and has no turbidite (bottom of Fig. 12e). Dome-shaped deep water fan bodies of grain flow origin usually exhibit a clinoform configuration with low frequency and strong amplitude reflections because of the existence of thick and porous sands (Saller et al., 2004) (Fig. 10a). Due to the thin sandstone layer, the sedimentary body of turbidity current usually shows the hummocky configuration of medium amplitude and frequency (Berg, 1982; Posamentier and Kolla, 2003). Sedimentary bodies of debris flow genesis often exhibit chaotic configuration (Cukur et al., 2012).

Non-sedimentary bodies usually have a similar outline in different directions, characterized by an antiform outline and blanking of internal reflections. Mud diapirs occur mainly in the mud-rich zones of sedimentary basins (Sun et al., 2012) (Fig. 10b). Eruptive bodies occur in an area of intense magmatic activity. Gas chimneys usually occurs in young rifting basins that have abundant deep gas sources, and are characterized by a top bright spot, internal low frequency, blanking or weaker reflections compared with the surrounding area, and bottom-downward bending (Horozal et al., 2009). Residual hills are developed usually on a large unconformity, and their internal configuration is similar to the surrounding formations beneath the unconformity (Xu et al., 2005). A low-amplitude volcanic cone with a 'limestone cap' and inner chaotic reflection is difficult to distinguish from a reefal structure based on seismic reflections alone (Badley, 1985). However, it can be distinguished by the low interval velocity features of the internal volcanic agglomerate (see Fig. 21). A large volcanic cone is characterized by granulated reflections of the core and laminar convergence reflections toward the wings, the hummocky-shaped strong amplitude reflections at the top of the cone are the seismic response of multi-stage lava layers (Xu et al., 2021) (Fig. 10b).

3.2.4.2. Internal configurations of sheet or sheet drape reflectors. The internal configurations corresponding to the sheet or sheet drape reflectors (Fig. 10c) are usually parallel, and occur in the shelf, gentle ramp, abyssal plain, and other open and flat seafloor environments (Mitchum et al., 1977a, 1977b), dominant seismic lithofacies is shale interbedded with siltstone.

3.2.4.3. Internal configurations of bank-shape reflectors. The internal configurations corresponding to bank-shape reflectors are parallel oblique and shingled seismic reflections (Fig. 10d) and both of these clinoforms develop in shallow-water environments. The parallel oblique configuration indicates the existence of mouth bar sands in a fluvial-dominated delta, whereas the shingled configuration indicates the existence of coastal bars in a wave-dominated delta (Berg, 1982).

3.2.4.4. Internal configurations of wedge-shape reflectors. The internal configuration corresponding to the wedge-shape reflectors is convergent (or divergent). The wedge-shaped bodies can be divided roughly into two major categories, namely, a *syn*-depositional wedge in a half-graben basin and a shelf-edge foreset wedge (Fig. 10e). The former can occur anywhere in a rift basin, where coarse-grained facies such as sandstone usually developed on the fault side, while mudstone and siltstone facies occur in the tilted uplifted zone. The latter occur on the edge of the shelf or platform. The slope of the shelf-margin wedge developed in the period of highstand is usually gentle, and this wedge is typically argillaceous, with the weak-amplitude clean reflections converging toward the basin (Figs. 8 and 10e). The wedges developed in the periods of rapid sea-level fall and during lowstands can be sand rich, where the sands are mainly distributed in the top and bottom flat reflections of the wedge, with the weak clinoform reflections still within the mud layers.

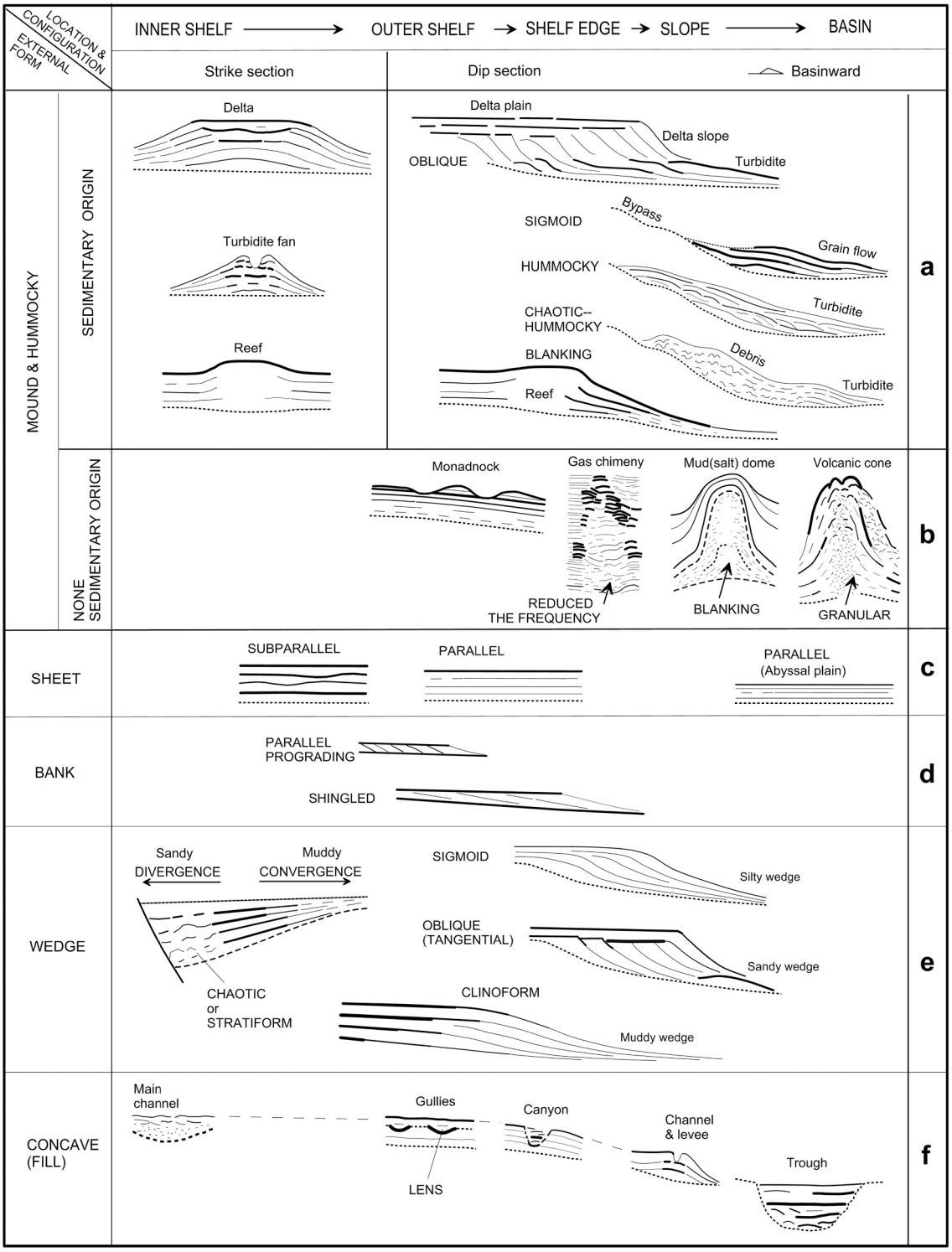

Fig. 10. Seismic stratigraphic configuration and facies distribution patterns, showing the relationship between external form, internal configuration, location and section orientation (summarized from Bubb and Hatlelid, 1977; Sangree and Widmier, 1977; Berg, 1982; Badley, 1985; Haq et al., 1987; Galloway and Hobday, 1996; Posamentier and Allen, 1999; Stow and Mayall, 2000; Nilsen et al., 2007; Catuneanu et al., 2009; Xu et al., 2013, 2015; Wang et al., 2019; Matenco and Haq, 2020; Xu et al., 2021). Image height and width indicate relative dimensions of sedimentary bodies; sequence boundaries plotted as dotted lines, while solid lines indicate reflection features; line width denotes amplitude; solid lines and dashed lines denote continuity.

3.2.4.5. Internal configuration of incised valleys. Incised valleys can take many forms, such as main channel, gullies, canyon, channel and trough (Prather et al., 1998) (Fig. 10f). The internal reflections of a thick sand body deposited in a main channel is usually seen as chaotic or blanking reflections (see Fig. 14a), which is the seismic response of the sandstone fill sequence peculiar to the main channel (Shanley and McCabe, 1994). The sand body in the shelf-edge gullies is usually seen as an outline of a lens with right-downward skew-symmetrical strong wave reflections (Chen et al., 2015; Rankey, 2017). The channels located at the top of retrograding turbidite fans (slope fan in lowstand systems tract) are

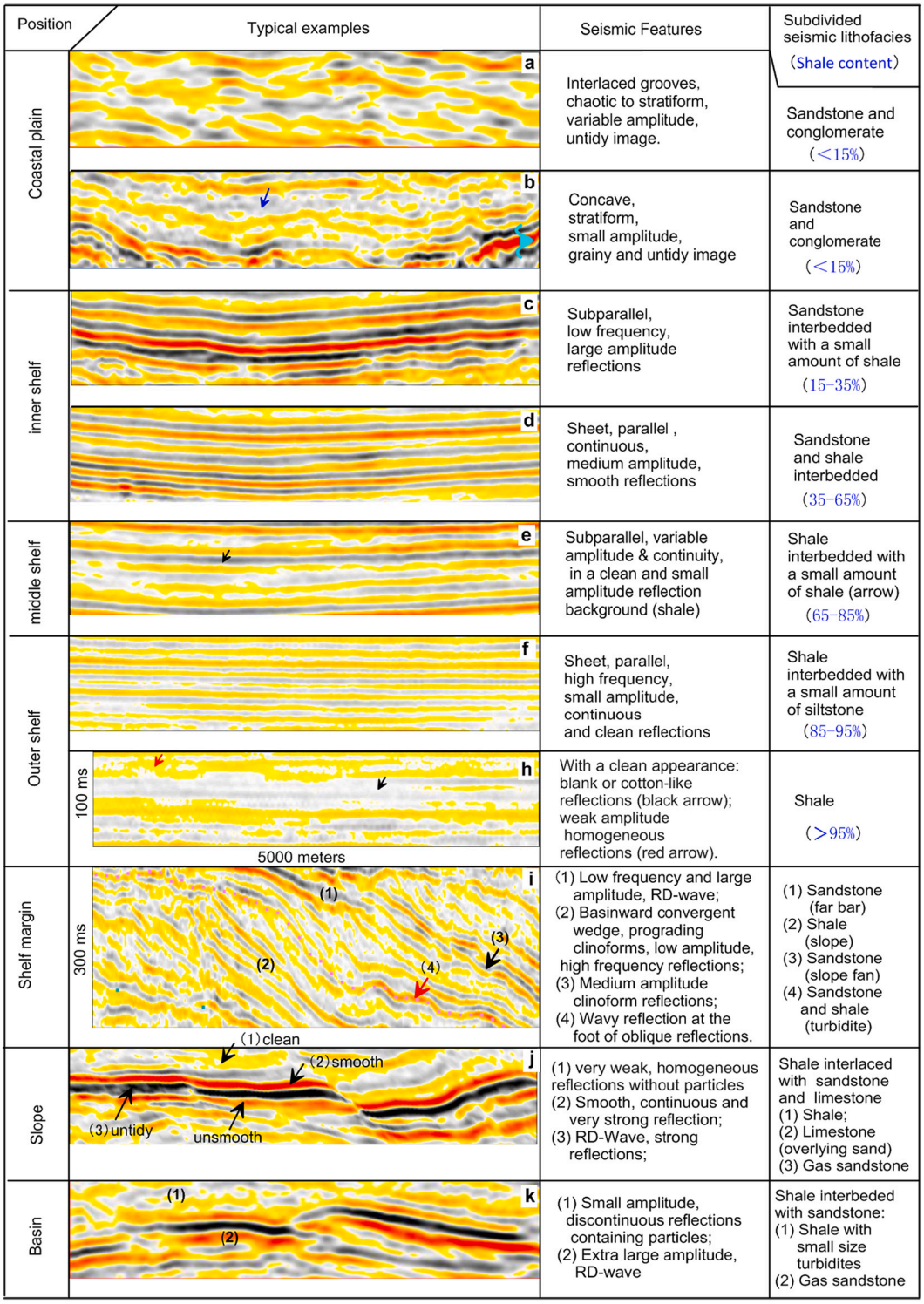

Fig. 11. Profiles showing various seismic lithofacies in siliciclastic sediments. General seismic reflection characteristics of clastic seiments are shown in a passive continental margin basin setting. All the images are from the continental shelf of northern South China Sea, with zero-phase and American polarity displayed, and gain control amplitude of 80; the section length is 5 km, time thickness is 300 ms for image i, and 100 ms for all others (after Xu et al., 2021).

usually filled with mudstone and seen as blank reflections, whereas the channel sands in the fan show up as short and strong amplitude events (Berg, 1982) (Fig. 10f). The internal configuration of a canyon is mainly onlapping fill of parallel or hummocky configurations, in which the downward skew-symmetrical strong wave reflections represent porous channel sands (Gong et al., 2015). The plane combination of "gullies-canyon-channel" (Stow and Mayall, 2000) is seen in Fig. 16a.

3.3. Amplitude and frequency

3.3.1. Amplitude

The amplitude of a seismic reflection wave mainly reflects the contrast in acoustic impedance at the interface of the thick layer or the difference of lithology. It is dependent largely on the lithology, porosity, pore-filling media (see Fig. 21), and the thickness of the sandwich or the

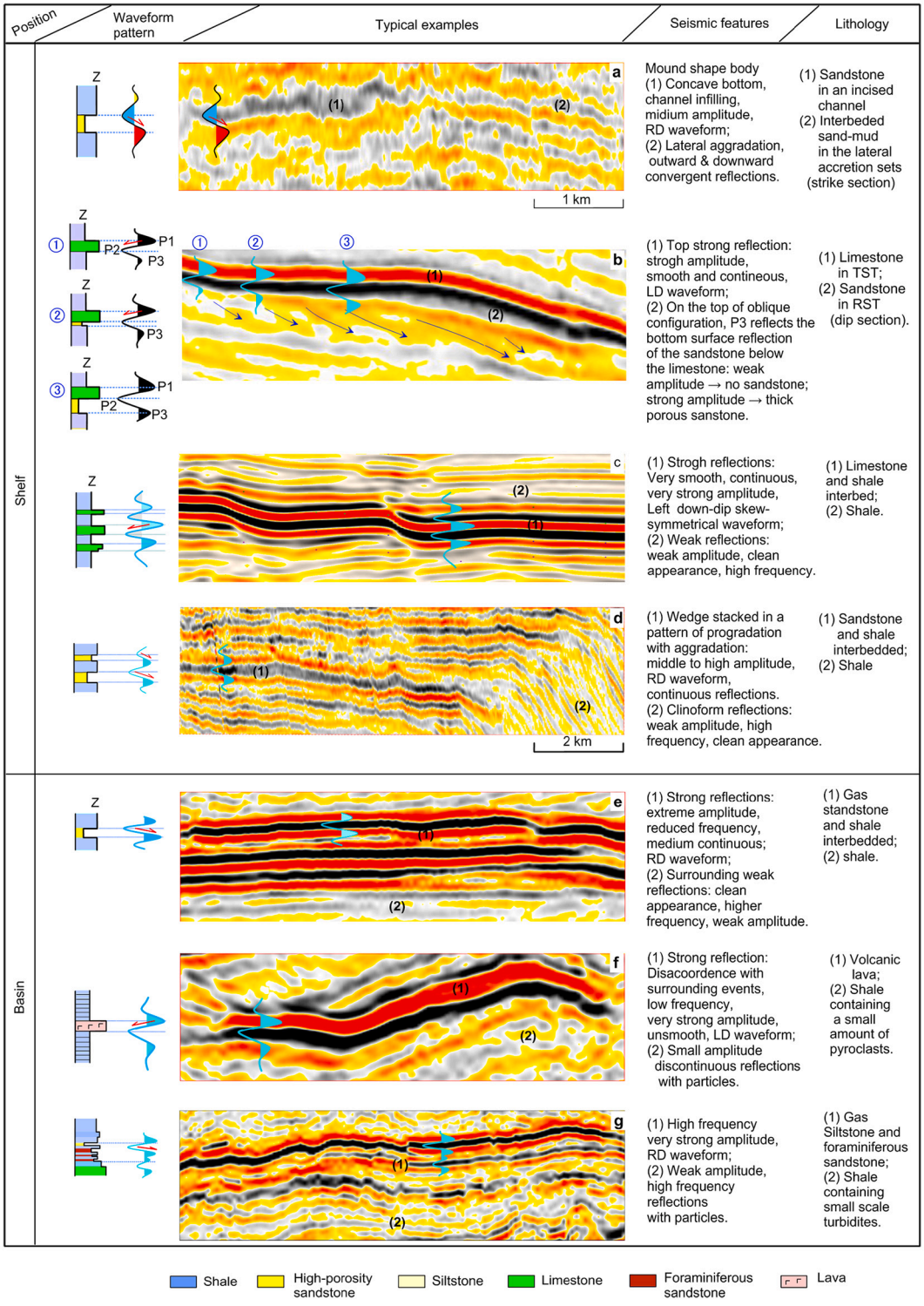

Fig. 12. Special seismic lithofacies (Oligocene, Baiyun Sag, data courtesy of CNOOC Shenzhen Branch). All seismic profiles are from the continental slope in northern South China Sea, with zero-phase and American polarity displayed, gain control amplitude set at 80, section length of 5 km except for image d (10 km), and time thickness of 300 ms. The smoothness and continuity of image d are inadequate owing to horizontal compression and layer flattening. Most of the waveforms shown are from the seismic records near a borehole, and the lithology profile is from the borehole data that have been simplified.

spacing between two thin layers (e.g., Anstey, 1980; Badley, 1985; Brown, 2011; Wang et al., 2015; Zeng, 2018). The geological properties of amplitude can be summarized by the following four aspects:

(1) The interfaces of sand and shale usually generate a reflection with low to medium amplitude (Fig. 11a, b, d, e, i), but extremely large amplitude reflections can be generated at the top and bottom of an interlayer of high porous sandstone at shallow depth and/or gas-saturated sandstone (Figs. 11j, k; 16 e, g);

(2) Coal, undercompacted mudstone, and high-porosity gas sand are of abnormally low velocity, whereas calcareous sandstone, limestone (Fig. 12b and c), and basalt (Fig. 12f) are of abnormally

high velocity. The interfaces between each of these two types of lithologies and normal clastic rock will produce extremely large amplitude reflections;

(3) For sandstone or limestone encased in shale, the amplitude of the composite wave varies with the lithological thickness (thin beds here are those less than a quarter of a wavelength thick) (Figs. 4a);

(4) The reflection amplitude of a set of thin sand-shale interbeds is proportional to the accumulated thickness and is not related to the number of thin layers. However, there is a limit, i.e., to a total interlayer thickness of less than ~ λ/4.

The reflection amplitudes of conventional seismic sections are all relative and are usually distinguished at four levels, i.e., extra-large, large, medium, and small (Fig. 13a and b). To clearly distinguish the relative amplitudes of these four levels, it is usually necessary to reduce the gain-control value of amplitude of seismic reflections on the workstation to below 80. However, to distinguish a relatively large amplitude reflection against a weak amplitude background, such as that of gas-bearing dolomite in a large setting of compact carbonate rock (Fig. 13b), the gain control value of amplitude must be adjusted to above 200 in order to measure the amplitude variation of the reflection of the porous dolomite.

3.3.2. *Frequency*

The term 'frequency' in seismic facies analysis is the dominant frequency, which refers to the number of reflection events per unit time (Badley, 1985) and indicates the lithological changes in the vertical direction (Wang, 1991). If the vertical changes in lithology (e.g., sand/shale; limestone/shale) are extremely frequent, there will be numerous reflection events. As a rule the sedimentation rate decreases from the shelf toward the slope and basin, and basinward there is also a decrease in the thickness of isochronous stratigraphic units (Fig. 11a–f). In the slope and basin areas, sandy debris-flow sediments are reflected at low frequencies because of the large thickness of the monolayer (Figs. 11j, k, 12e), whereas turbidites are reflected at high frequencies because of the thinness of the monolayer (Fig. 12g).

Other exceptional circumstances can reduce the apparent frequency. For example, bright spots are usually seen as relatively lower frequency features (Fig. 15b), caused mainly by a local increase in sand thickness and the extended duration of a low-velocity layer (Brown, 2011). A gradient layer of acoustic impedance causes the corresponding lobe to widen and the apparent frequency to decrease (Fig. 5). For this reason, the fattening waveform generated by the gradient layer of wave impedance is also called the low-frequency waveform (Anstey, 1980).

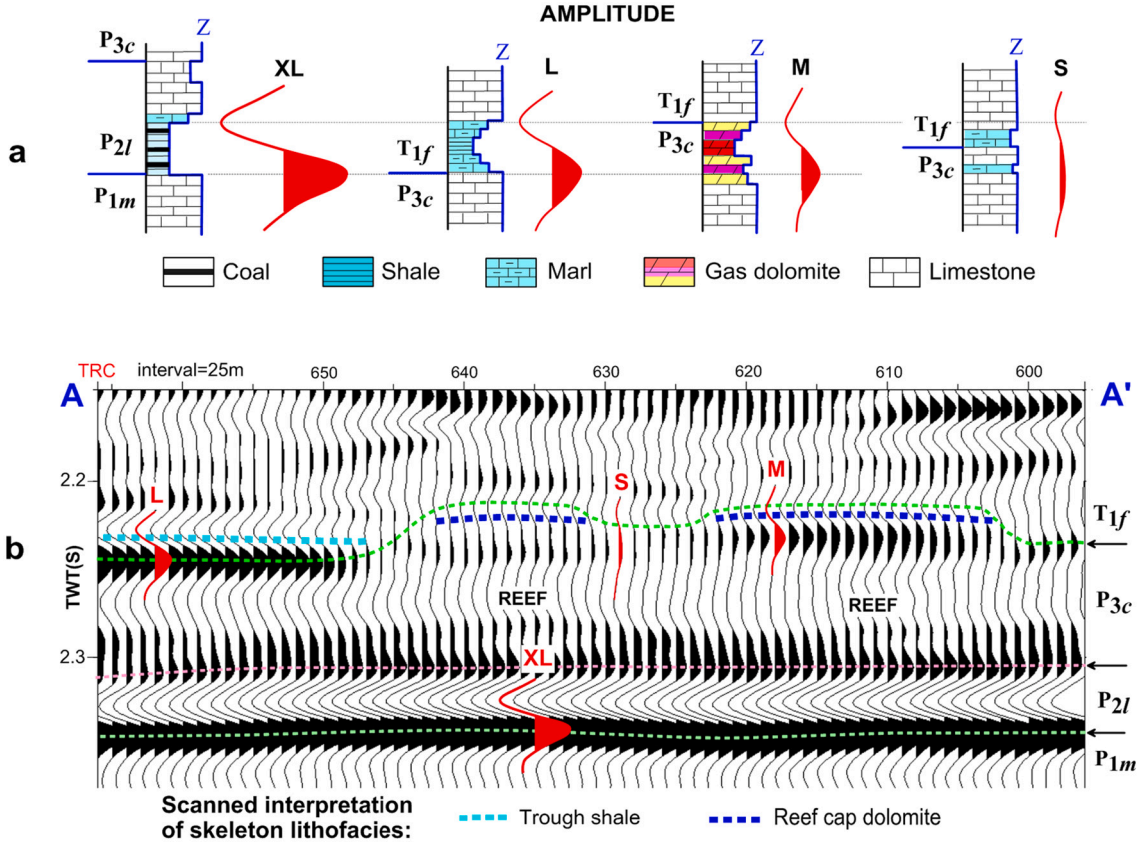

Fig. 13. Seismic reflection amplitude of different wave impedance structures or rock type combinations (Permian, Sichuan Basin, data courtesy of Petrochina Southwest Oil and Gas Field Company). a. Four levels of relative amplitude are displayed. The curves on the right side of the lithological columns are the macroscopic acoustic impedance curves obtained from the nearby borehole data. The interlayers of coal and shale, shale and marl, gas-bearing dolomite, and muddy limestone are all low-impedance layers, and the difference of wave impedance is obvious compared with the high velocity layer of tight limestone. The amplitudes of the composite wave generated by the top and the bottom reflections of these four low speed layers are extra large, large, medium, and small, respectively. b. Paleozoic platform-edge reef seismic profile. Zero-phase and American polarity are displayed and gain control amplitude is set at 80. The coarse dotted line reflects the relatively low-velocity strata, the shallow blue line reflects the shale and mudstone developed in the trough area, and the deep blue line reflects the reef cap dolomite. Both coastal coal-bearing shale and shale in the trough are developed in a low-energy environment, their formation structure is laterally stable, and seismic reflection presents a smooth, continuous, and neat appearance. A reef-cap dolomite develops in a high-energy environment (high-energy beach) and its stratigraphic structure is unstable horizontally, resulting in changes in waveform and amplitude of adjacent seismic traces, showing poor smoothness and continuity of the events. (For interpretation of the references to colour in this figure legend, the reader is referred to the web version of this article.)

3.4. Continuity and smoothness

Continuity of the seismic event reflects the stability of the distribution of the formation in the horizontal direction (e.g., Mitchum et al., 1977a, 1977b; Roksandic, 1978). Smoothness of event denotes the flatness of an impedance-contrast interface (Sheriff and Margaret, 1980) and the horizontal homogeneity of the medium. Generally, events generated by stratal interfaces of fluvial facies are unsmooth and discontinuous. Events generated by sheet sand and other interfaces that have been flattened by waves show up as relatively smooth and continuous. Events generated by a marine limestone interlayer usually has optimal smoothness and continuity (Fig. 12b and c). In many instances, the seismic reflection characteristics of volcanic lava layers (Fig. 12f) and limestone layers (Fig. 12c) are similar, except for smoothness. Therefore, the smoothness parameters can be used to distinguish between limestone and volcanic lava layers (Xu et al., 2021).

3.5. Waveform (special pattern)

There are three basic waveform patterns, including the symmetrical, skew-symmetrical, and low-frequency waveforms (Fig. 5). A typical symmetrical wave (zero-phase wavelet, Fig. 5a) occurs most often at the interfaces of the seafloor (Fig. 2b), the top and bottom interfaces of thick limestones, the basement (in the bottom right corner of Fig. 11b) and the like. In many cases, the lower side lobe of the symmetrical wave can be deformed by the overlying pulses from other underlying interfaces (such as the bottom surface of a limestone layer, when only the upper side lobe and center lobes are preserved, Fig. 12b). The display polarity of seismic data (European or American polarity) can be diagnosed by a complete or incomplete symmetrical wave from the seafloor and other geological boundaries with large impedance contrast.

A right-downward skew-symmetrical wave (RD-wave) is generated by a low-impedance interlayer encased in shale or carbonate, such as gas sand (Fig. 5b) or gas dolomite (Fig. 13a). A left-downward skew-symmetrical wave (LD-wave) is caused by a high-impedance interlayer (such as limestone or basalt) encased in siliciclastic strata (Fig. 12c and f). After determining the sedimentary body by traditional seismic parameters, an RD-wave can be used to directly identify the sandstone with large porosity, e.g., main-channel sandstone (Fig. 12a), mouth bars, sheet sandstone (Fig. 12d), channel sandstone (deep-water sandstone, Fig. 11k), and superposed fan sandstone (Fig. 12e) in a deltaic and deep-water fan sedimentary system. A dolomite reef-cap reservoir (Fig. 13) can be recognized directly from the conventional seismic data. An LD-wave can be used to identify a volcanic lava layer (Fig. 12f), limestone layer (Fig. 12c) and the like (Xu et al., 2021).

A low-frequency asymmetrical wave (Fig. 5d) is caused by a transition layer with gradual impedance change. The thickness of the transition layer is usually less than ~λ/4, because if it were much greater than this thickness, the low-frequency event (wide complex lobe) is separated into two events (Fig. 4b). This can be used to diagnose the sedimentary trend and the vertical grain size variation, as well as a weathering-crust reservoir.

3.6. Appearance

The appearance of the seismic profile describes the feature resulting from the lateral small-scale changes of stratigraphic structure within a thick lithologic intervals with similar acoustic impedance (thick layer) (Wang et al., 2015; Xu et al., 2021). It is similar to the concepts of roughness of a plane view (Posamentier et al., 2007) and waveform dissimilarity of adjacent traces (Qi et al., 2016; Majid and Mohammad, 2017).

Terms such as irregular, untidy, dirty, particle, particles, homogeneous and compact, neat, clean are used to describe the appearance of seismic profiles (Fig. 14). The murky appearance derives from rapid and minor changes in the wave shape and the amplitude of seismic events, and is not caused by random permutations and combinations of seismic events, which is what distinguishes it from chaotic reflections (Fig. 15).

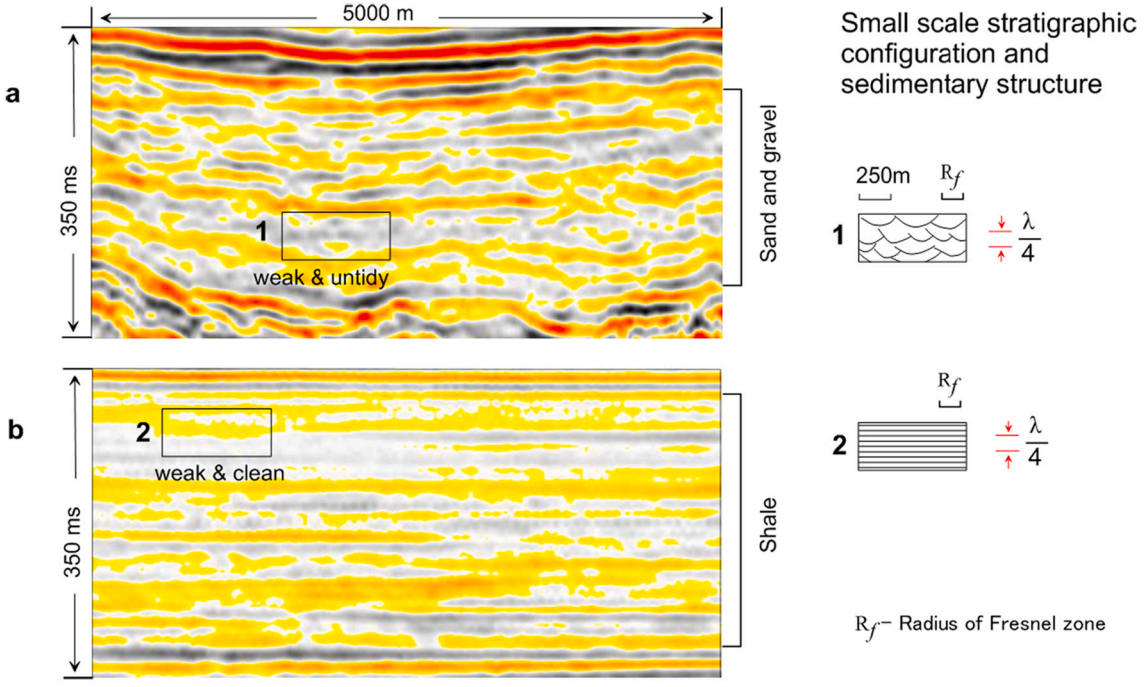

Fig. 14. Appearance of reflections in siliciclastic settings (after Xu et al., 2021). Zero-phase and American polarity are displayed. Because of a lack of a strong-wave impedance interface in the large set of sandstones (a) and shales (b), the resulting image is composed of weak-amplitude reflections. Because of the development of sandstone in a high-energy environment, the lateral small-scale stratigraphic structure (wave impedance structure) is unstable, thereby showing an irregular and untidy appearance (a). Mudstone is developed in a low-energy environment, the lateral stratigraphic (wave impedance) structure is stable or changes regularly, thereby producing a clean appearance (b).

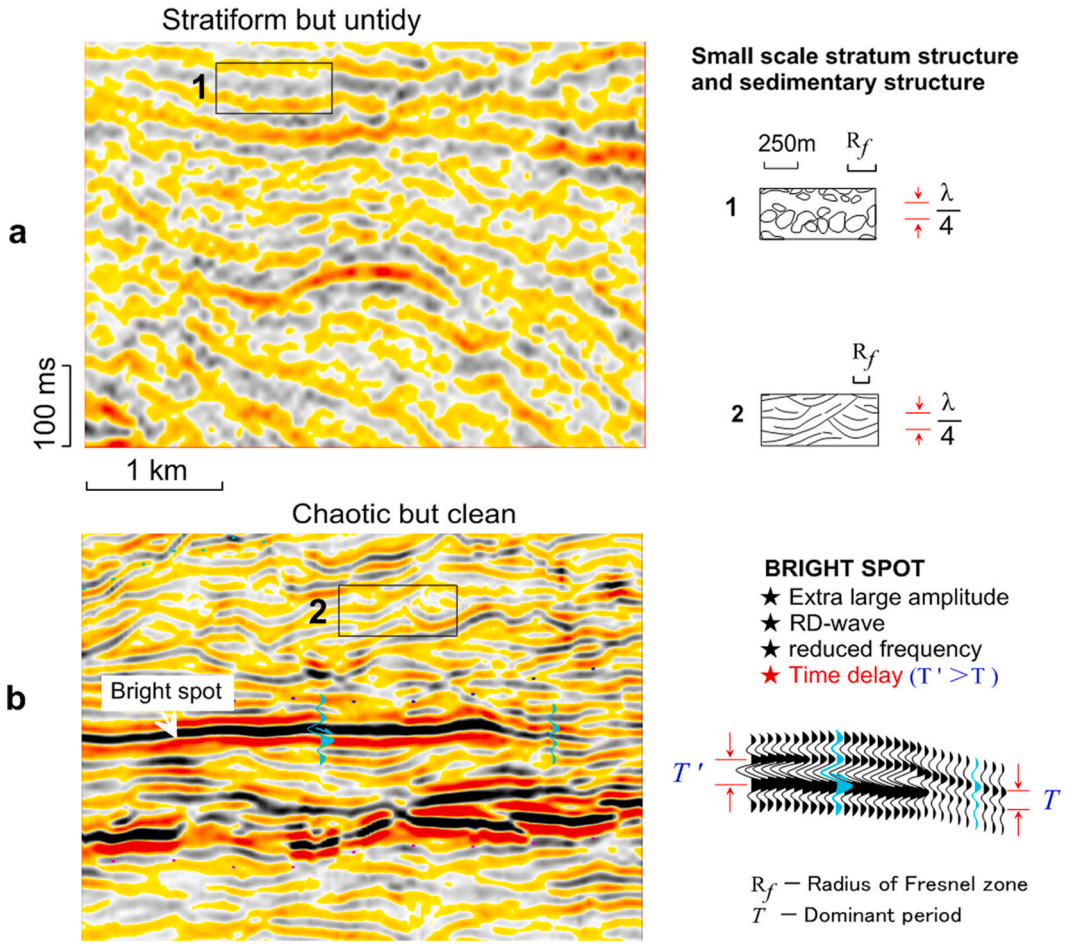

Fig. 15. Difference between a chaotic configuration and appearance and the key elements of a bright spot (Miocene, Baiyun Sag, data courtesy of CNOOC Shenzhen Branch). Zero-phase and American polarity are displayed. a. Stratiform configuration and untidy appearance (pyroclastic sedimentary rock at the flank of a volcanic cone). b. Chaotic configuration and clean appearance (channel deposits on a continental slope). Four elements of the bright spot: extra-large amplitude, RD-wave, reduced frequency, and time delay are indicated.

Geologically speaking, an untidy appearance is caused by lateral mutations of a small-scale stratigraphic structure (such as trough cross-bedding in a channel, Fig. 14a) or material composition (such as mixed pyroclastic rocks, Fig. 15a) in the thick layer. If the lateral variation of small-scale stratigraphic structure and material composition in the thick layer is extremely stable horizontally (such as shale deposited in a standing water environment), the seismic amplitude and wave shape of the seismic events are stable, it shows a clean appearance (Fig. 14b).

Small-scale stratigraphic structures are those that have a height less than $\lambda/4$ and a width that is less than the radius of the Fresnel zone (Fig. 14). Large-scale stratigraphic structures produce various seismic reflection configurations, including chaotic ones, and the small-scale structural interfaces only weakly change the shape and amplitude of reflection waves but do not produce reflection events (Xu et al., 2021).

The appearance parameters are mainly used to identify large sets of single lithologic seismic lithofacies, such as large sets of sandstones, mudstones and shales, pyroclastic sedimentary rocks, and the distinction between beach facies grainstone and open platform facies micrite. Large sets of single lithology all show weak amplitude reflection inside, but they show different appearance because of their different small-scale formation structure.When sandstones and grainstones are deposited in shallow-water high-energy environments, the small-scale impedance structure can frequently change laterally, presenting an unclean appearance and granulated reflection (Fig. 14a). The formation structure of mudstone and micritic limestone is laterally stable and shows clean appearance (Fig. 14b). Because of the uneven distribution of pyroclasts, the seismic reflection of pyroclastic sedimentary rocks has a untidy and dirty appearance (Xu et al., 2007), with many small fragments scattered randomly (Fig. 15a).

3.7. *Other parameters: bright spot, size, thickness and curvature*

Bright spot reflection is a comprehensive parameter which contains several independent sub-elements. In previous studies, strong amplitude, dipole phase and horizontal dot reflection were mainly used to identify bright spot (Anstey, 1977, 1980; Badley, 1985). Xu et al. (2015) proposed that the bright spot should be determined by four elements (Fig. 15b): strong amplitude, frequency reduction (trough broadening and loop area increasing), right drown-dip skew-symmetrical wave (equivalent to dipole phase), and time delay (caused by gas-bearing formation velocity reduction). In terms of testing for oil and gas, all four of these characteristics must be present simultaneously, but, in fact, the fourth is often overlooked.

Bright spots can be used to identify many important seismic lithofacies and sedimentary microfacies. For example, the main channel, mouth bar and coast bar sandstones are prone to bright spot reflection due to their high porosity and low wave impedance, especially when the sands contain hydrocarbons. In addition, there are relatively low-velocity interlayers that can also produce bright spot reflections. Examples include peat and coal beds occurring in a bog environment, gypsum intercalations in carbonate rocks, and undercompacted

mudstone beds deposited in the center of the depression. The fourth marker is important because it can be used to identify the false bright spot produced by limestone and shale interbedded at the top of an uplift (such as volcanic cone).

Size and thickness are two less commonly used geometric parameters (Badley, 1985; Brown, 2011). Curvature is a geometric parameter derived from sedimentary landform (Di et al., 2018). These three parameters play an important role in the identification of some special sedimentary bodies. For example, The seismic reflection characteristics of the volcanic cone and tower reef are very similar, but there is a significant difference in size. Volcanic cones can often reach heights of thousands of meters, while tower reefs are usually only a few hundred meters high.

3.8. Plan view seismic image

Plan view seismic images (Posamentier et al., 2007) of seismic facies can be obtained by seismic slicing, scanned interpretation of skeleton lithofacies (Xu and Pang, 2021; Xu et al., 2021), and auto-classification of seismic facies units. These different types of plan geometric images can reflect the external contour and internal structure of the sedimentary body (Fig. 16) in simple geological conditions, which makes the plan image become an important parameter for seismic facies analysis, especially in seismic geomorphology and seismic sedimentology (Brown, 2011; Miall, 2016).

The plan view geometry of the sedimentary body is manifested mainly by the skeletal lithofacies bodies (Berg, 1982). In other words, the geometric features or depositional elements on the amplitude slice are actually a picture of the skeletal lithofacies (Brown et al., 1982; Posamentier and Kolla, 2003; Posamentier et al., 2007). As the amplitude is affected by the rock type combination, acoustic impedance difference, thickness, porosity, pore filling medium, and other factors, in many cases, the geometric image on the amplitude slice can be quite different from that of sedimentary facies, this is a major challenge in slice image analysis. The seismic scan interpretation method uses nine independent seismic parameters (Fig. 7) to determine the skeletal lithofacies in the seismic profile, so that the its generated skeleton lithofacies distribution map can more accurately reflect the skeletal distribution than the seismic slice image because it has eliminated the influence of overlying strong reflection and true or false bright spot reflection by seismic lithofacies identification. We suggest the study of sedimentary facies and sedimentary systems by scanning interpretation of plan views when complex lithofacies conditions are present.

4. Schemes of seismic facies analysis

So far the present, seismic facies analysis schemes can be classified into four categories, i.e., traditional, enhanced seismic lithofacies, slice image, and auto-classification. The traditional approach, developed in the 1970s, has been applied in various fields of subsurface geology, particularly stratigraphy and sedimentology. Seismic slice image analysis started in the 1980s (Brown et al., 1982), seismic geomorphology and seismic sedimentology in the 1990s (e.g., Mutti and Normark, 1991; Zeng et al., 1998), and automatic classification in the 1990s (Barnes, 1994; Addy, 1998; Coleou et al., 2003). However, detailed seismic lithofacies analysis is a new scheme developed in the last decade. These

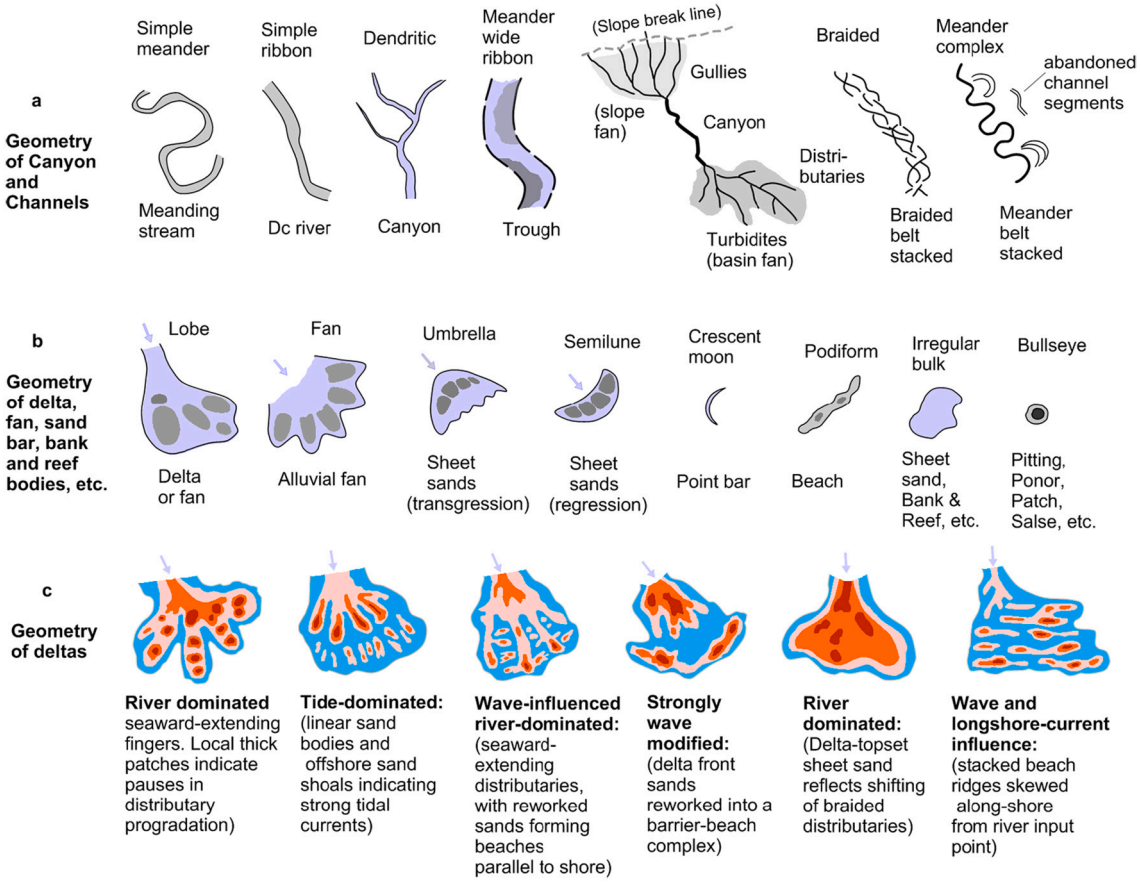

Fig. 16. The plan view geometry of the sedimentary body. a. Summarized from Stow and Mayall, 2000; Posamentier et al., 2007; Brown, 2011; Miall, 2016. b. Summarized from Brown, 2011; Zeng, 2013, among others. The arrows reflect the direction of the source. c. Different colors represent thickness of the sand layers. The thicker the colour, the thicker the formation (modified from Coleman and Wright, 1975; Miall, 2016). (For interpretation of the references to colour in this figure legend, the reader is referred to the web version of this article.)

four schemes are designed to meet different research objectives and accomplish different seismic facies analysis tasks (Fig. 17).

4.1. Traditional seismic facies analysis

In the traditional seismic facies analysis, six commonly used seismic parameters are used to classify seismic facies units and interval velocity was used to estimate seismic lithofacies. Sedimentary facies inferences are obtained by two steps (Mitchum et al., 1977a, 1977b; Sheriff and Margaret, 1980): (1) using the geometry, seismic attribute and relevant geological identification such as paleogeomorphology to classify the major seismic facies units; (2) converting seismic facies units into sedimentary facies units through borehole calibration or detailed seismic geological analysis. This working procedure has been widely used for decades, but its effectiveness is increasingly questioned because the accuracy of sedimentary facies obtained by traditional seismic facies analysis is too low to meet the requistes of modern exploration.

In the longer-term practice, it is found that there are two engrained limitations in the traditional seismic facies analysis (Xu et al., 2021). The first is its modest capability for lithofacies identification. With the traditional method major sedimentary environments can be recognized by such indicators as the external geometry and internal configuration of sedimentary bodies. While seismic attributes, such as amplitude, frequency, and continuity can sometimes be used to subdivide lithofacies. For example, the short events with low frequency and variable amplitude can indicate sand-mud interbed in a delta-plain environment, and the weak clinoform reflections can indicate shale in a prodelta environment (Berg, 1982). Nevertheless, it is extremely challenging to differentiate the thick flood-plain mudstones and thick channel sands because of their similar inner 'blanking' of reflections. Challenges related to continental margin facies are also encountered. For example, it is difficult to differentiate gas sandstone, gas siltstone, gas foraminiferal sandstone, limestone, and basalt layers because of their similar reflections, with low frequency and strong amplitude (Chen et al., 2015). Interval velocity is sometimes considered indicative of lithofacies, but it is not an adequate indicator as it can differentiate only the broad lithofacies categories (Badley, 1985), such as shale-prone or sand-prone deposits (Mitchum et al., 1977a, 1977b; Xu et al., 1990). Another disadvantage is that in the absence of ground-truthing from drilling data, geological processes that create various facies cannot be well understood with traditional seismic facies analysis. Sometime such disadvantages can be remedied by integrated seismic and geologic studies (provided that sufficient drilling data are available), but areas with limited borehole data or complicated geologic settings can yield ambiguous results with traditional seismic facies analysis (Fig. 18a).

4.2. Enhanced seismic lithofacies analysis

In order to overcome the limitations of traditional seismic facies analysis and improve the detail, Xu et al. (2021) proposed an enhanced seismic lithofacies analysis scheme. In this method, three seismic parameters reflecting rock types are added to enhance the capability of

Schemes / Features	Traditional seismic facies analysis	Enhanced seismic lithofacies analysis	Seicmic slice image analysis 1) Seismic geomorphology 2) Seismic sedimentology	Auto-classification of seismic facies
Key Parameter	1) Position; 2) External form; 3) Configuration; 4) Amplitude; 5) Frequency; 6) Continuity.	1-6) T*P(traditional parameters);* 7) Smoothness; 8) Appearance; 9) Waveform; 10) Provenance.	1-6) *TP;* 7) Plane geometry of the slice of seismic parameters such as amplitude, coherence and acoustic impedance.	1-6) *TP;* 7) Wave shape; 8) Polarity; 9) Derived attributes of AVO, amplitude, curvature, etc..
Key Technology	1) Wavelet processing; 2) 3D seismic; 3) Impedance inversion; 4) High resolution; 5) 3D visualizations.	1-5) TP; 6) Original form restoration; 7) Waveform analysis; 8) Lithofacies identification; 9) Scanned interpretation; 10) Sedimentary systems reconstruction (new)	1-5) TP; 6) 90° phase shift; 7) Spectral decomposition; 8) Stratal slicing.	1-5) TP; 6) Neural network pattern recognition; 7) Machine learning.
Preliminary results	1) Distribution map of seismic facies units: Properties of reflector; Paleo-current, etc..	1) Environment; 2) Skeleton lithofacies; 3) Flow path.	1) Slice images: Depositional elements; Paleo-current, etc..	1) Sesmic facies map: distribution of seismic facies units.
	Convert ↓ Calibration; or/and Integrated interpretation	Deduce ↓ Superposition analysis of three elements	↓ Calibration; or/and Integrated interpretation	↓ Calibration
Final results	Sedimentary facies with very rough lithofacies and flow path	Sedimentary systems including environments, lithofacies, and flow paths	Seismic slice that label or delineate depositional elements (e.g., subfacies, microfacies, sandstone body, reef, etc.)	Seismic attribute map that labal or delineate geological bodies (subfacies, micro-facies, sand body, reef, salt dome, etc.)
Thresholds of application	No limitation	Data: no limitation; Knowledge: fundamentals of seismic geological interpretations	Data: 3D seismic data; simple lithological condition; local block; sufficient borehole data Knowledge: geophysics, mathematics, geology	
Task (in oil and gas)	**Recognization of unknown things** (Identification and description of sedimentary bodies with unclear geological properties)		**Description of known things** (something with known geological properties, such as channel sand body, reef cap dolomite reservoir, etc.)	

Fig. 17. Comparison of four working schemes of seismic facies analysis.

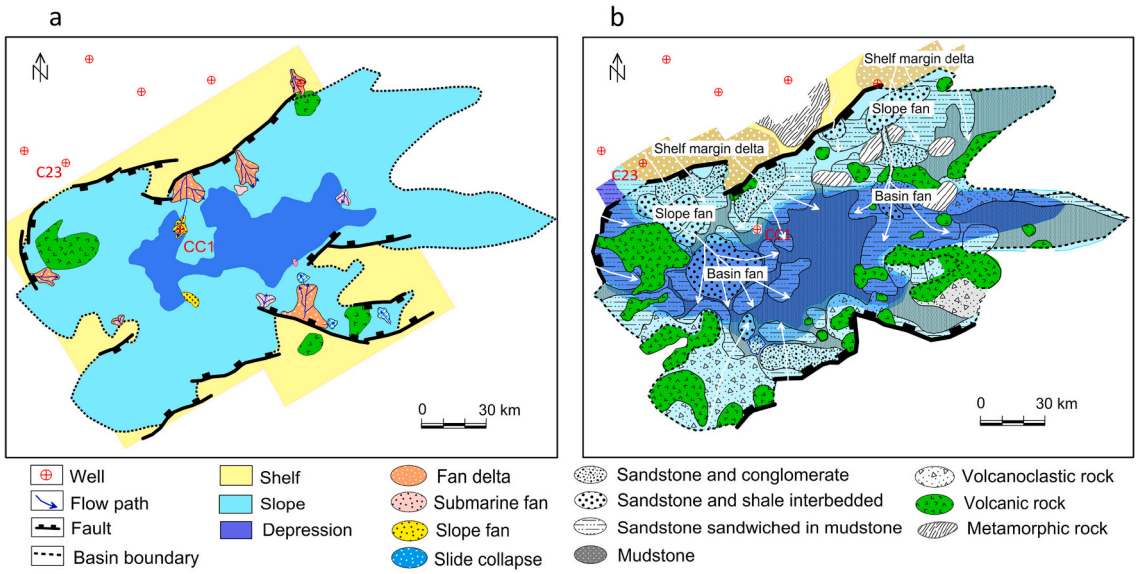

Fig. 18. Comparison of sedimentary facies maps made by traditional method (a) and detailed lithofacies method (b) (modified from Xu et al., 2021), both of which show the sedimentary systems of lingshui Formation of upper Oligocene in Xisha Trough Basin, SCS.

lithofacies identification, and the sedimentary system with high precision is reconstructed by the superposition of three sedimentary elements (i.e. lithofacies, environment and hydrodynamic conditions). The scheme has been applied to more than ten basins in Asia, including back-arc, carbonate platforms, large lake, cratons, passive continental margin and active continental margin basins (Figs. 18b), and has been found useful byexplorationists (e.g., Chen et al., 2015; Guo et al., 2021).

4.2.1. Key techniques

Enhanced seismic lithofacies analysis encompasses several new techniques, among which there are five key procedures: seismic profile recovery of the original stratigraphic structure, waveform (special pattern) analysis, detailed seismic lithofacies identification, scanned interpretation of skeletal lithofacies, and Reconstruction of depositional system by the superposing method (Fig. 19).

4.2.1.1. Restoration of the original structural seismic profile. The original structural profile of the sedimentary sequence can be restored through a process of segmented line-drawings of seismic events, reassembly, and modification (; Wang et al., 2019). This technique can restore the complete internal structural morphology and sedimentary landform of the sedimentary bodies (such as shelf-edge delta, slope fan, and basin fan, etc., Fig. 20), provide estimates of the paleo-water depth, and lead to an understanding of the development and distribution of the sedimentary facies and environment (Guo et al., 2021; Xu and Pang, 2021).

4.2.1.2. Waveform(special pattern) analysis. Waveform analysis is a technique to identify the combination of rock types based on the basic principle of "specific seismic waveform corresponding to specific acoustic impedance structure" (Liu, 1997; Wang et al., 2015). Waveform analysis includes three sub-techniques: 1) Analysis of velocity variation with depth for different rock types (Fig. 21); 2) Matching analysis of phase, amplitude, and waveform between synthetic seismogram and seismic record near the borehole. Waveform analysis can be performed only after the phase, amplitude and waveform between synthetic seismogram and seismic record have been matched more than 80% (Luo, 1999); 3) Composite waveform analysis based on three basic waveforms. See Xu et al. (2021) for four examples and composite waveform analysis in 4.4.1.

Waveform analysis can dates back to the 1960s (Ricker, 1953; Widess, 1973; Anstey, 1980). However, it has not received much attention in the years until 2010s, when the definition and display of polarity were often confused (Liu, 1997; Brown, 2011). As a result, waveform analysis technique has remained underappreciated. In recent years, Xu et al. (2021) have further improved the technique as apart of their enhanced seismic facies analysis. Waveform analysis is now an important basis for seismic lithofacies analysis, especially in frontier basins lacking well data.

The reflected waves in seismic profiles are mostly composite waves formed by the superposition of reflected waves generated by many interfaces, rather than special waveforms. Therefore, some geophysical researchers have questioned the utility of waveform analysis. In fact, gas-bearing sandstone and limestone interlayer produce standard RD-wave (Figs. 11k-(2), 12e-(1), 15b) and LD-wave (Fig. 12b-(1)), respectively; When limestone and gas-bearing sandstone combine, a combination of two specific waveforms will be produced (Xu et al., 2021). Thick, gas-free pore sandstones also appears as a relatively low-velocity layer, producing RD-waves with weak to strong amplitude (Fig. 12a-(1) and (2); 12d-(1)). These major skeletal lithofacies can be identified by waveform or waveform as the main parameter. For thin sandstone bodies with poor porosity, although they do not produce special waveforms and cannot be identified by waveform, they produce special seismic responses of interbeds of sandstone and mudstone, which can be determined by seismic lithofacies analysis. In addition, we do not need to know the thickness and specific depth domain location of these subordinate skeletal lithofacies, but need to determine whether they exist in a certain location for the purpose of detailed seismic lithofacies analysis.

4.2.1.3. Detailed seismic lithofacies identification techniques. Enhanced seismic lithofacies analysis improves lithofacies resolution by adding three markers that were not commonly used before. These three newly added markers (smoothness, neatness and waveform) and six commonly used markers in traditional seismic facies analysis (position, external shape, external configuration, amplitude, frequency and continuity) constitute a total lithofacies identification index system. Detailed seismic lithofacies can also be identified with such a system even when drilling data is not available in the study area (Xu et al., 2021). For example, nine subdivided seismic lithofacies can be identified in northern area of South China Sea: sandstone, sandstone interbedded with a small amount of shale, sandstone and shale interbedded, shale interbedded with a small amount of sandstone, shale, pyroclastic sedimentary rocks, volcanic agglomerate, volcanic lava, thin layer limestone

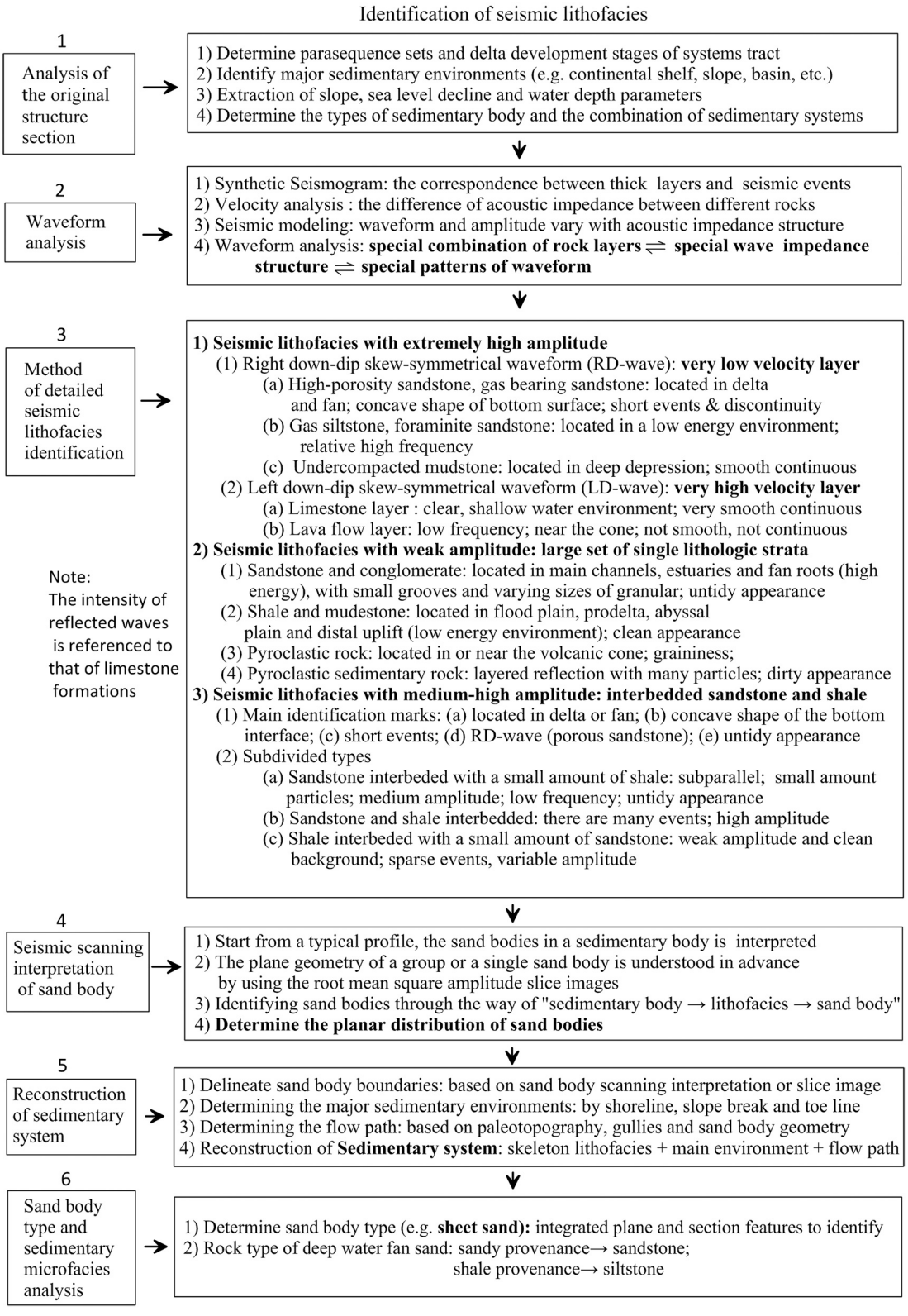

Fig. 19. Flow chart of detailed seismic lithofacies analysis for passive continental margin basin

(Figs. 11, 12, 15). Supported by original structural profile recovery and waveform analysis techniques described above, subdivided seismic lithofacies identification techniques can be applied to detailed lithofacies prediction in different basins, including in basins with a variety of rock types and few drilling data (Xu et al., 2021). Fig. 19 shows in detail the process and method of subdividing the seismic lithofacies.

4.2.1.4. Scanned interpretation of sandstone (skeletal lithofacies). The sand body scanned interpretation method was first proposed in the late 1990s and it successfully depicted sand body boundary in the Tertiary lacustrine strata of Junggar Basin (Luo, 1999). Since then the technique has been used for routinely discerning stratigraphic traps (Wang et al., 2004). Such scanned interpretation of lithofacies refers to the

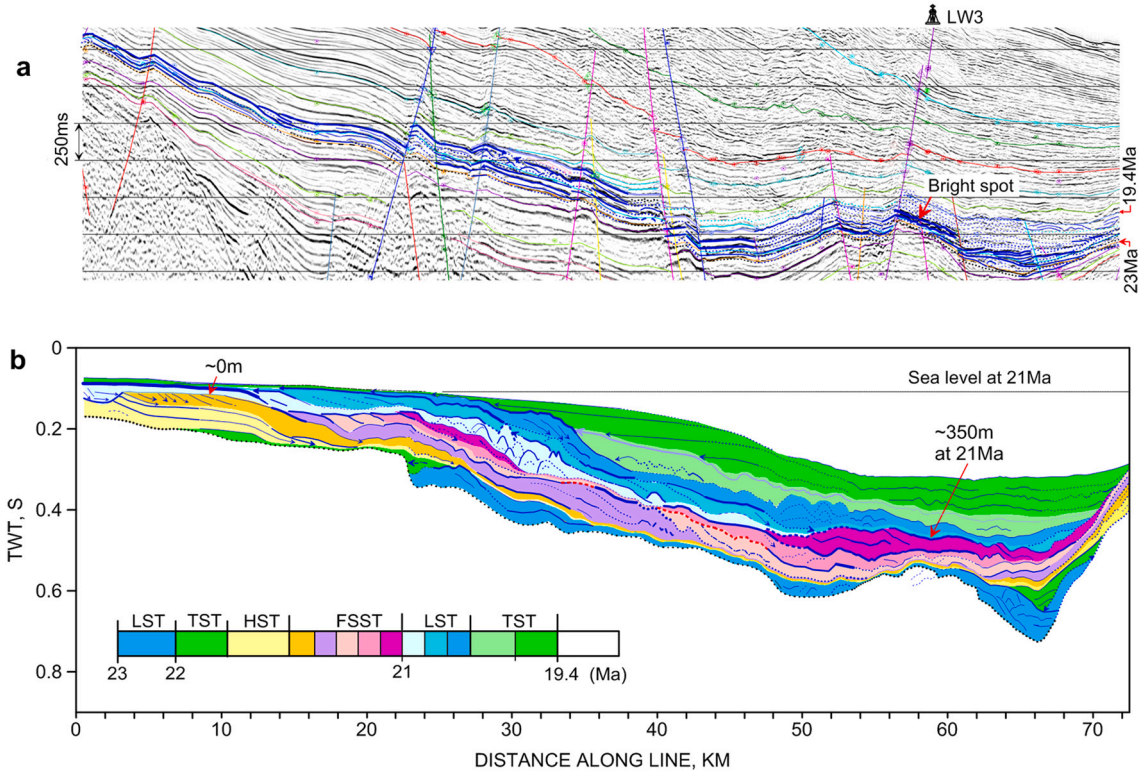

Fig. 20. An example of restoration of the original depositional section (Baiyun Sag, northern South China Sea, modified from Wang et al., 2019). Zero-phase and American polarity is displayed. a. Seismic stratigraphic and structural interpretation with line-drawing of the interval of interest; b. Sedimentary sequences restored after seismic interpretation, in which line thickness represents reflection strength of event amplitudes, dashed and solid lines indicate event continuity, and arrows indicate the termination of reflections. Estimated paleo-water depths is indicated for prominent surfaces at 21 Ma (SB) and at 18.5 Ma (MFS and SB). Abbreviations: LST — lowstand systems tract; TST — transgressive systems tract; HST — highstand systems tract; FSST — forced regressive systems tract.

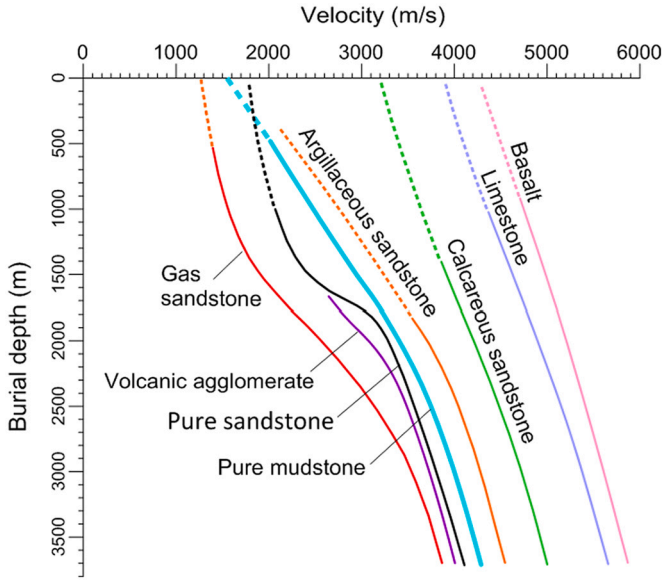

Fig. 21. Dependence of Tertiary rock velocity on buried depth in Baiyun Sag (modified from Anstey, 1980, Brown, 2011 and Xu et al., 2021). Thirty-two wells were drilled in the Baiyun-Liwan Sag and the buried depth is measured with reference to the seafloor. (For interpretation of the references to colour in this figure legend, the reader is referred to the web version of this article.)

continuous mapping of a certain skeletal lithofacies in one direction in a three-dimensional seismic block (Xu and Pang, 2021). This technique can not only accurately delineate the boundary of the skeletal lithofacies such as sand body, but also detect the connectivity between different sand bodies (Fig. 22a). This method can also be used to describe the distribution of sand bodies in 2D seismic profiles (Xu et al., 2021) (Fig. 18b).

4.2.1.5. Reconstruction of sedimentary systems by superposition of lithofacies, environment and flow path. A sedimentary system refers to three-dimensional (3D) lithofacies assemblages that are genetically related in terms of environment and sedimentary processes (Fisher and McGowen, 1967; Zhu, 2003; Jiang, 2010; Miall, 2016). Xu et al. (2021) proposed a new method of superimposing three elements of depositional system to reconstruct the depositional system, i. e., lithofacies + environment + channels, to arrive at a picture of the depositional system.

The lithofacies here refers to skeletal lithofacies, which are determined by scanning interpretation. In the siliciclastic strata, the sandstone is the skeletal lithofacies and the argillaceous rock is the matrix lithofacies. In the carbonate basin, basin shale and marl, lagoonal marl, reef-cap dolomite and granular rock are all skeletal lithofacies, while the platform micrite is a matrix lithofacies. Matrix lithofacies are background lithofacies and do not require scanning interpretation. The sand body scanning interpretation projects the sand bodies in an isochronous stratigraphic unit such as a systems tract onto a plan (Fig. 22a). However, these sand bodies were developed in stages during the progradation sequence, but the sandstone layers in the same sand body are considered to be deposited at the same stage (Fig. 22b). After the scanning is completed, the boundaries of each sandstone body can be delineated (the upper half of Fig. 22a), and then the sand bodies are roughly classified by the estimation of their thickness, porosity and area size (step 6 in Fig. 19). For example, in the SQ2–3-FRST of Eocene in the Baiyun Sag, South China Sea, the sand bodies are roughly divided into two categories: good porosity sand body and poor porosity sand bodies

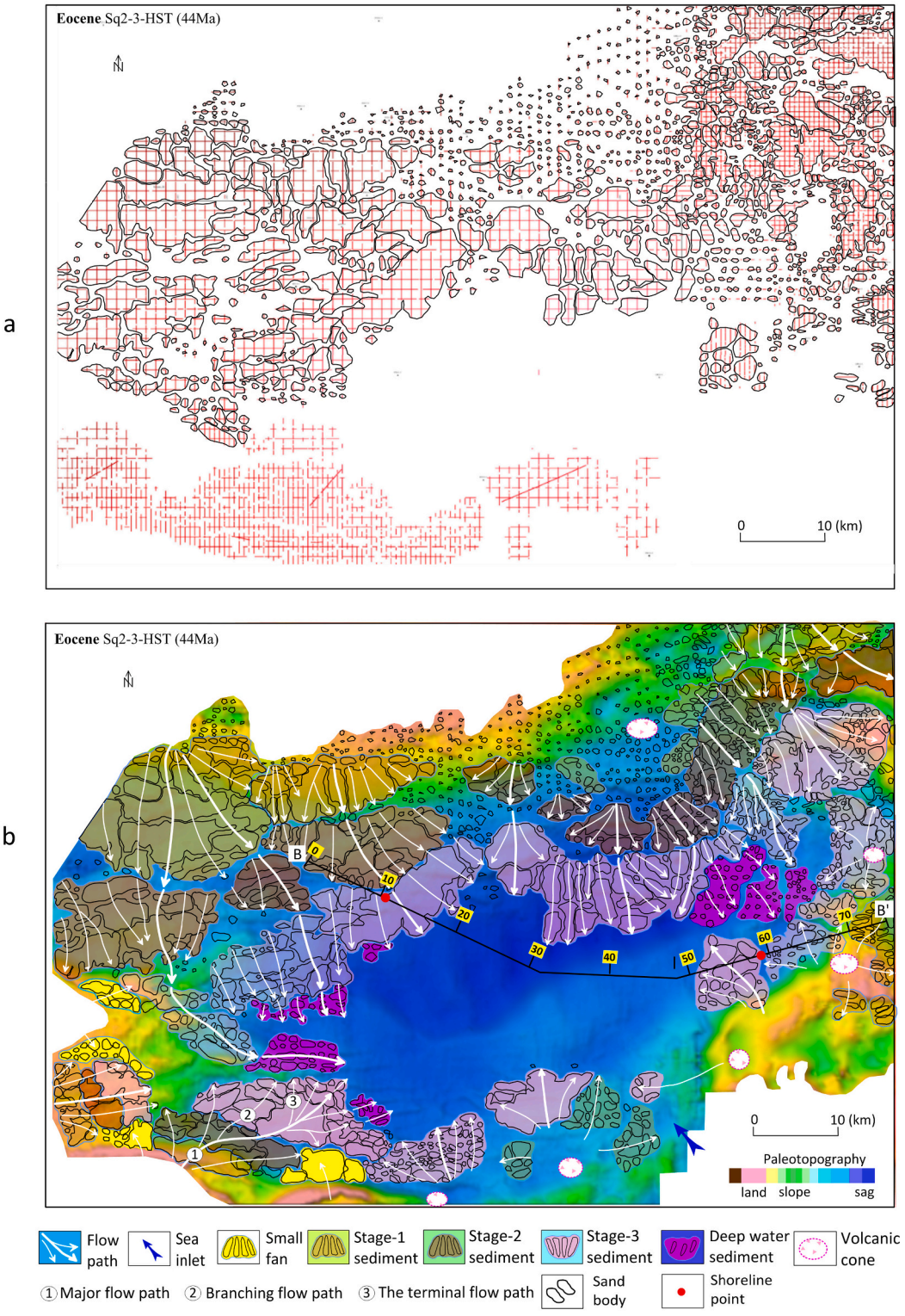

Fig. 22. Sand body distribution and flow path system map (Eocene, ~44 Ma, Baiyun Sag, modified from Xu and Pang, 2021). a. Sand body distribution map obtained by sand body scanning interpretation; no sand boundary delineation was done in the southern area in order to display the original sand scanning interpretation image. The sand bodies were first superimposed on the paleogeomorphic map, and then, according to the assemblage characteristics of the sand bodies and the sequence of the development of the sand bodies (observed from the original-form structural section), the boundaries of the individual sedimentary bodies were delineated and the sedimentary periods were divided. Braided river deltas and fan deltas are developed in the northern and western slope zones of the sag, and the strata is stacked in a pattern of descending progradation, which makes the deltas or fan lobes of the three stages developed separately. Whereas in the southern and eastern fault sub-sag areas, nearshore subaqueous fans are developed, and the strata are mainly stacked in a pattern of aggradation, and only the sedimentary bodies in the last sedimentary stage can be seen.

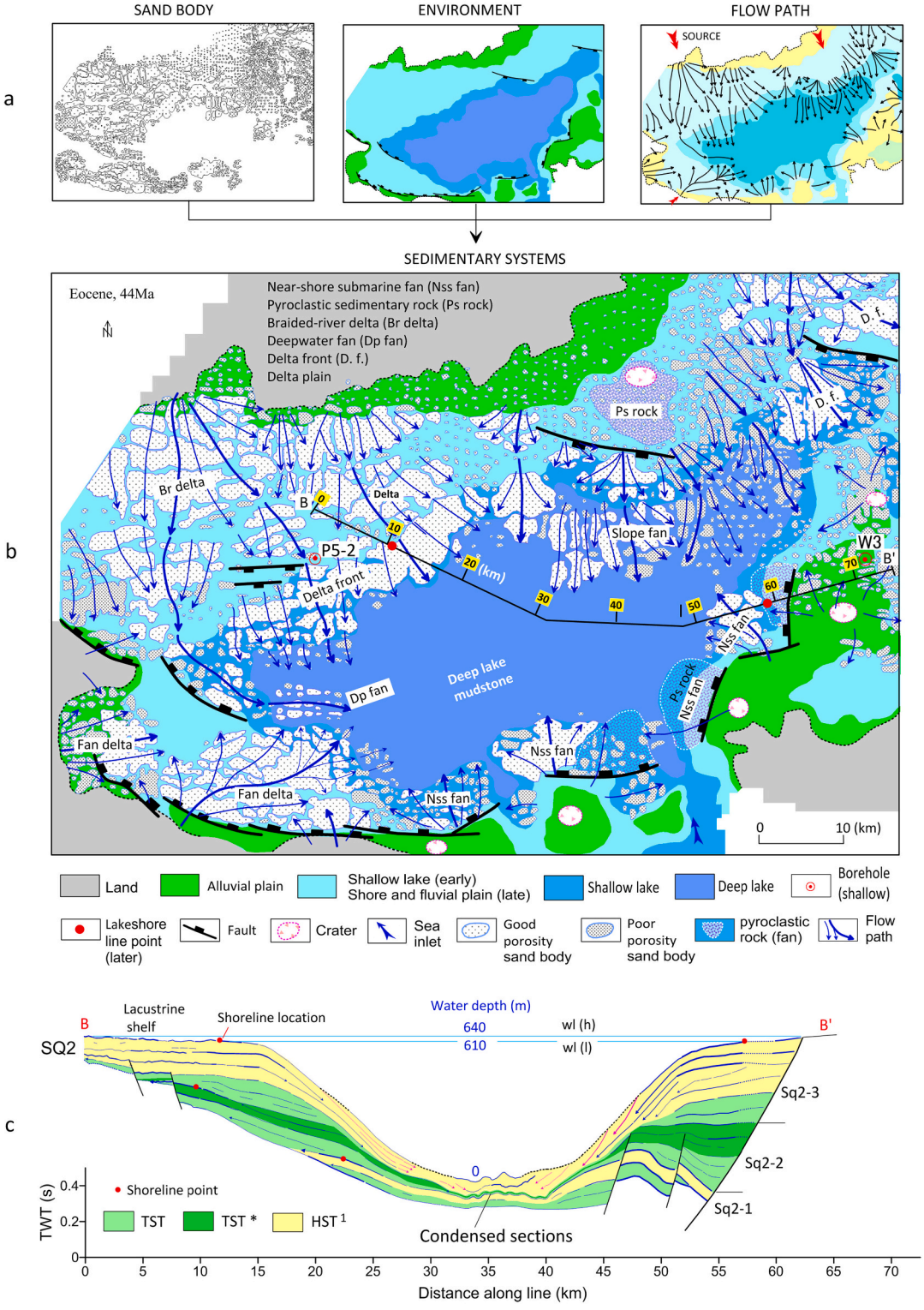

Fig. 23. Sedimentary facies map reconstructed by superimposing skeleton lithofacies, main sedimentary environment and flow path (Baiyun Sag, northern South China Sea, modified form Xu and Pang, 2021). a. Sedimentary facies map. Braided river deltas are developed in the Northern Slope of the sag, fan deltas are developed in the western fault terraces, nearshore subaqueous fans are developed in the southern and eastern fault depression areas, and deepwater shale and a few deepwater fans are developed in the center of the sag. The northwest, southwest and northeast of the sag are mainly siliciclastic sedimentary areas; the eastern part of the northern slope is a mixed siliciclastic and volcanic-clastic deposition area; and the southeast is dominated by pyroclastic deposits. b. SQ2 original-form structural seismic profile. SQ2 is a composite sequence composed of three third-order sequences; in the SQ2–1 and SQ2–2 sedimentary periods, the base of the basin was sank rapidly and the strata stacked in a pattern of retrogradation, resulting in only one type of genetic stratigraphic unit developed in the two sequences; HST unit was developed in late SQ2–3, forming lacustrine shelf and large lake basin; a large number of deep water shale and mudstones (high quality source rocks in condensed sections) are developed in in the central area of the basin.

(Fig. 23b).

Major environment here refers to the categories of broad environmental regions within the sedimentary system, e.g. fluvial, shelfal, slope and basin environments. They may be interpreted using seismic data and by delineating coastlines, depositional knick-lines, and boundaries of deep water lithofacies, etc. (Xu et al., 2021) (Figs. 18b and 23a).

The flow path in river dominated delta is composed of four elements: main flow channels, branch flow channels and terminal flow channels and the flow direction. Major flow paths can be outlined by connecting the erosional grooves and valleys observed at the tops of mound-shaped sedimentary bodies with channels and submarine canyons observed on adjacent seismic lines. Branching flow paths can be mapped by connecting "sand bodies" or other sedimentary bodies that are transported by water flow in the dip direction. The terminal flow path is determined mainly by the plan geometry and geological properties of a single sand body or group of sand bodies (Fig. 22b, fan delta in the south). The direction of the flow is determined by the progradational structure and the paleotopography, and the palaeotopographic map is best constructed from a thickness map of stratigraphic units that fill the entire basin. Attention should be given to the relationship between thicknesses of the strata and paleo-water depth, because their relationship differs in compensated and under-compensated sedimentation conditions (e.g., Kirk, 2016; Gutiérrez-Paredes et al., 2018). In nearshore subaqueous fans and braided streams and deltas, distributary channels fan out (upstream) or converge (downstream), and the main channel may not be particularly pronounced (Fig. 22b).

After the three components (i.e. the skeletal lithofacies, the main environment, and the main flow path) are completed, they are superposed together (Fig. 23a). Then, based on the geometric images of the sand body, environment and main flow path information, branching flow paths can be constructed, and a complete flow path system can be established (Fig. 23b). The sand bodies and their associated depositional bodies connected by the same flow path system are grouped within the same depositional system. Sedimentary facies in a depositional system are determined according to the geometry of sand bodies and other skeletal facies bodies as well as sedimentary environment and flow path they located.

4.2.2. Application prospects and limitation

Enhanced lithofacies analysis helps researchers obtain more geological information from seismic data. With the wide application of various interpretation softwares in the 21st century, people can more quickly and easily observe and interpret the subsurface geological world, including structures, stratigraphic configurations and sedimentary bodies. However, while interpretation software enables interpreters to obtain a large amount of seismic reflection information quickly and conveniently, the ability to transform seismic information into geological information is constantly declining (Brown, 2011). This ability decline of manual seismic interpretation may not be a problem in areas with abundant drilling data; but when drilling is sparse or data is not available, this becomes a serious limitation because software interpretation results that are not calibrated to well data are less than meaningful. Shell Oil Co. and PetroChina, for example, have conducted more than a dozen deep-sea drills deep in the South China Sea over the past decade (Chen et al., 2015; Madon et al., 2015). The design drawings and data provided by the researchers were fascinating, but ultimately failed due to inaccurate lithofacies predictions. In fact, the ability to obtain rock information directly from seismic data is thus an imperative not only for scientific studies such as marine geology but also for global climate change and mineral resource surveys, enhanced lithofacies analysis can help meet this need.

It should not be ignored that enhanced seismic lithofacies analysis also has its disadvantages (Fig. 18). First of all, more basic knowledge is required of researchers; basic knowledge of the combination of geophysics and geology (sections 2 and 3), mastery of the five techniques for enhanced seismic lithofacies analysis, and work experience are all essential. Secondly, recovery of the original structural profile and scan sandstone interpretation can be time consuming. Therefore, this method is more suitable for the study of unknown geological events, such as the study of sedimentary facies in the area with few wells, complex lithofacies and large area. Seismic slice analysis or wave impedance inversion is a better choice to describe the reservoir distribution of known sedimentary bodies. Third, as seismic facies analysis, the results of enhanced seismic facies analysis are qualitative, even though the technique can already identify sub-lithofacies types.

4.3. Seismic slice image analysis

Since the beginning of the twenty-first century, 3D-seismic data have been widely used in hydrocarbon exploration and exploitation and slice-plan seismic facies maps began to replace traditional seismic facies maps (e.g., Zeng et al., 1998; Posamentier and Allen, 1999; Posamentier, 2001; Posamentier and Kolla, 2003; Davies et al., 2004; Brown, 2011; Koša, 2015; Verma et al., 2018; Abbas et al., 2018; Zeng et al., 2018; Leila and Moscariello, 2019). Seismic slice imaging and analyses of sedimentary facies became the main method for seismic facies analysis (e.g., Posamentier, 2001; Brown, 2011; Zeng, 2018).

4.3.1. Seismic slice data

Seismic slices include amplitude slices, coherence slices, acoustic impedance slices, etc. (Posamentier, 2001; Posamentier et al., 2007; Chopra and Marfurt, 2012; Hart, 2013; Roy, 2013) (Fig. 24), where the amplitude slice data is the most commonly used (Brown, 2011). As mentioned previously, the main factors affecting the reflection amplitude are: the difference in acoustic impedance between skeletal lithofacies layer and matrix lithofacies layer; the thickness of a skeletal layer, and the spacing between two skeletal layers (Brown, 2011; Wang et al., 2015). When the formation structure is the same throughout and the acoustic impedance of the mudstone layer changes with depth, the amplitude is closely related to rock type, porosity, and matrix medium of the skeletal rock. In regions with shale-rich strata, such as the continental shelf edge, where there are only two rock types of sandstone and shale, the plan geometry of amplitude slices can effectively determine the boundaries and internal structure of the sedimentary body. Multitrace coherence can effectively reflect the lateral mutation of the stratigraphic structure, and is mainly used to determine the boundaries of organic reefs, channels, and other sedimentary bodies or *depositional elements* (Posamentier and Kolla, 2003). Acoustic impedance sections combined with rock sections are considered as appropriate petrographic analyses of seismic data (Brown, 2011). The image of wave impedance slice reflects the distribution of sand body, which is similar to the image obtained by sandstone scanning interpretation. However, due to the high precision of acoustic impedance data, they need to be constrained using large drilling datasets. They are mainly used to show the reservoir boundary and physical property changes and are not commonly used in seismic facies analysis. When all three kinds of data are available, a comprehensive analysis is useful for improving the accuracy of sedimentary facies analyses.

4.3.2. Key techniques

There are five key techniques used to support slice image analyses: isochronous seismic stratigraphic interpretation, selecting the appropriate interval or phase, horizontal and stratal slicing (Zeng et al., 1998) or proportional slicing (Posamentier et al., 2007), 90° phase shift, and spectrum decomposition (Partyka et al., 1999). The first two are general seismic slice image analysis techniques (Posamentier et al., 2007; Brown, 2011), while the last three are special processing techniques applied to seismic data that are also key techniques used in seismic sedimentology (Miall, 2016; Zeng, 2018).

4.3.2.1. Isochronal interpretation. Isochronal seismic stratigraphic

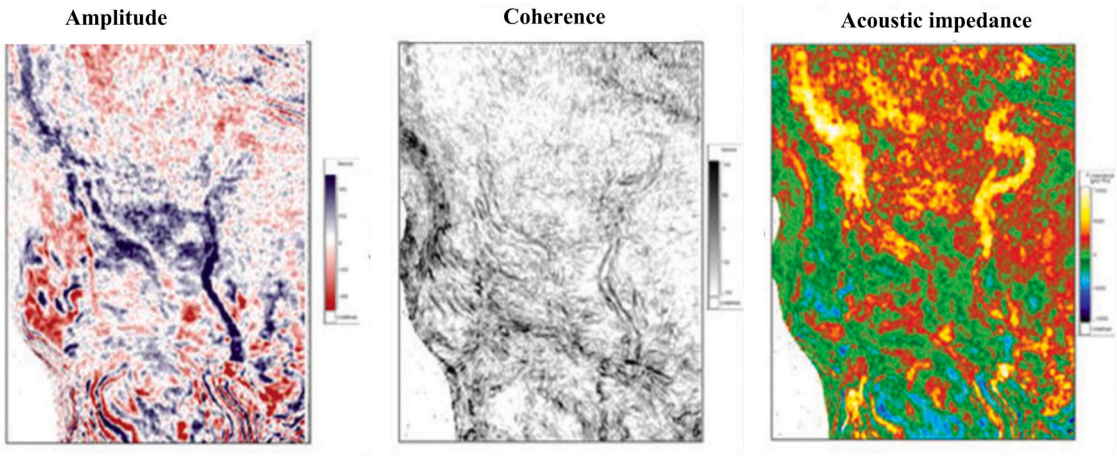

Fig. 24. Three examples of stratal slicing (modified from Brown, 2011). (For interpretation of the references to colour in this figure legend, the reader is referred to the web version of this article.)

interpretation is very important for seismic slice image analysis. In previous studies, most of the seismic slices that accurately reflect the geometry of the sedimentary body are seismic slices with carefully interpreted isochronous interfaces (Brown et al., 1982; Posamentier et al., 2007; Brown, 2011) (e. g., Figs. 25-27), while the unsuccessful cases are mostly related to the diachronous interpretation of reflections.

There are many reports on how to achieve isochronous stratigraphic correlation, we will not repeat them. Here we show a seemingly diachronous but in fact isochronus case (Fig. 13). A "reef cap" reservoir developed at the edge of the Late Permian Trough in Eastern Sichuan is one of the main gas reservoirs in the Sichuan Basin (Fig. 13c). Extensive drilling data (including paleontological correlation) and seismic calibration (e.g., Ma et al., 2007; Caineng et al., 2011; Li et al., 2015; Liu et al., 2016; Wu et al., 2017b; Zhou et al., 2017) show that in the trough area, the top boundary of the Changxing Formation is marked on the crest (corresponding to the bottom surface of the trough shale); while at the coral reef location, it is marked on the trough (corresponding to the top surface of porous dolomite); and in the inter-reef (or lagoon) area, it is again marked on the crest (corresponding to the bottom surface of muddy limestone). The reason why researchers interpret in this way is that shale and argillaceous limestone deposited in negative geomorphologic units (trough and lagoon) are the bottom strata of the Triassic Feixianguan Formation which were deposited after the destruction of carbonate platform (Wu et al., 2017a). Only by such an isochronal interpretation can the sedimentary microfacies and the development and distribution of reef cap reservoirs can be shown correctly on seismic slice maps. This is the key to effectively solve the problem that low amplitude reef and reef cap dolomite reservoir is usually difficult to describe.

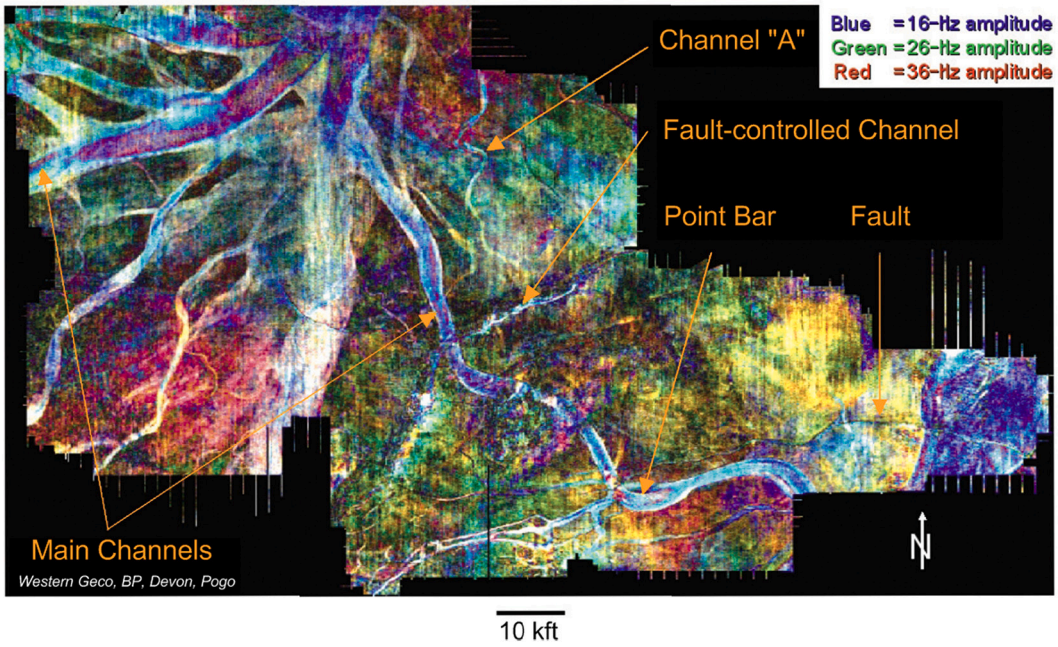

Fig. 25. Horizontal slice along a Pleistocene horizon from the Gulf of Mexico (modified from Partyka, 2005; Brown, 2011) showing amplitude in narrow frequency bands around 36 Hz as red, 26 Hz as green, and 16 Hz as blue. Such Red-Green-Blue blending provides a way to simultaneously view three frequency components. Note that the centers of the channels are predominantly blue, indicating increased sandstone thickness. If the velocity of the sandstone is 2000 m/s, the red, green, and blue represent sand bodies with thicknesses of ~14 m, 26 m, and 31 m, respectively, these are tuning thickness of three frequencies, i.e. thicknesses of $\lambda/4$. (For interpretation of the references to colour in this figure legend, the reader is referred to the web version of this article.)

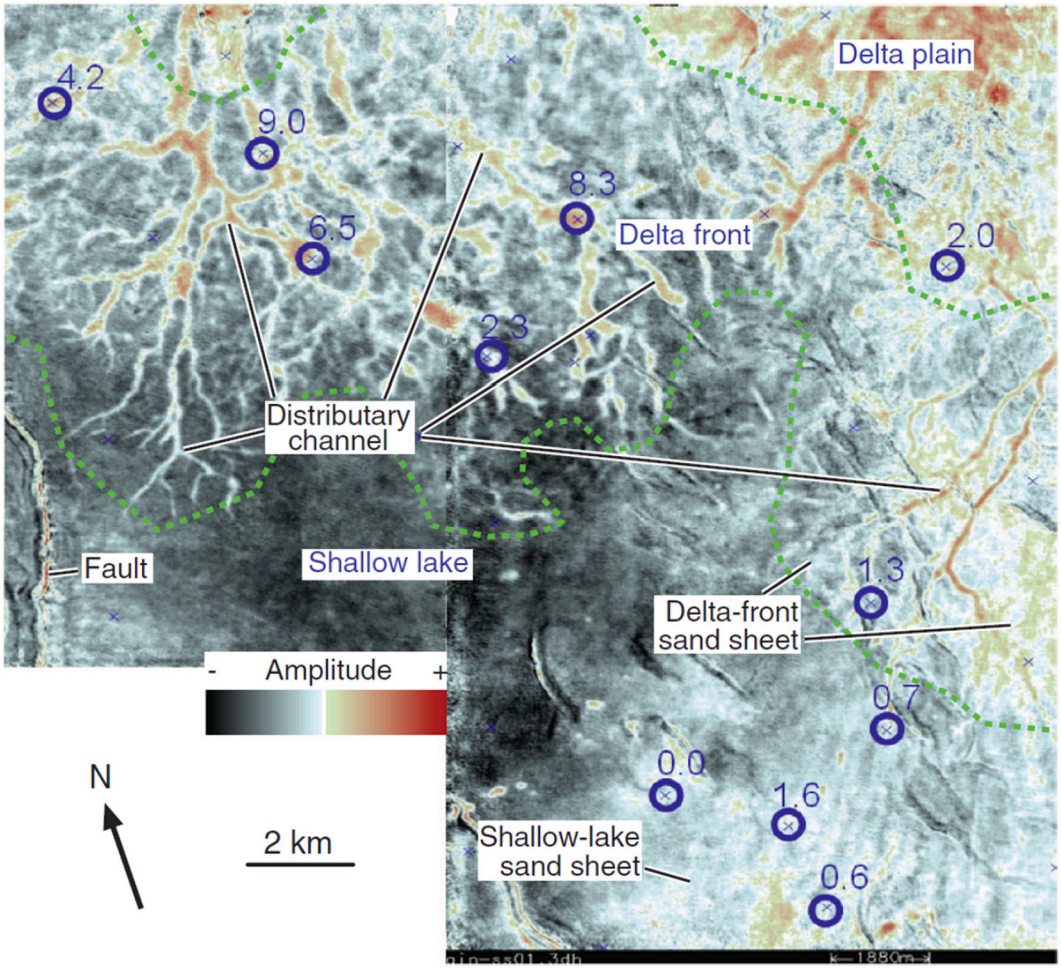

Fig. 26. Seismic amplitude slice in a shallow-water deltaic formation (modified from Zeng, 2018). Amplitude stratal slice made from 50 Hz dominant-frequency, −90° seismic data. The resolvable calculated horizontal limit (λ/4) is 10 ms (20 m). Thin distributory channels and sand sheets (in delta front and shallow lake facies) are composed of thin sandstone, but are different seismic landforms.

4.3.2.2. Phase selection. After the isochronal interpretation problem is addressed, how does one choose the appropriate phase for seismic slice analysis? For example, at the edge of the continental shelf, prograding deltas can often be covered by transgressive limestones (Fig. 12b). Such a sedimentary succession would produce a complex wave consisting of two to three large amplitude phases: Phase 1 (P1) is the main lobe of a zero-phase wavelet reflected from the top of the limestone; P2 is the composite main lobe reflected from the bottom of the limestone and the top of the sandstone; and P3 is composed of the reflected side lobe of the bottom surface of the limestone and the reflected main lobe of the bottom surface of the porous sandstone. The amplitude slices of the P1 and P2 phases will mainly reflect the development and distribution of shelf limestones. Only the amplitude of P3 can sensitively reflect whether a low-velocity porous sandstone layer is developed under the limestone. An amplitude slice of P3 can display the development of the prograding delta sands (Chen et al., 2015; Xu et al., 2021).

4.3.2.3. Time, horizon, and stratal slices. Time slicing can only reflect the plan view of sedimentary facies of near-horizontal strata, while slicing along target formations (horizon slicing) can reflect the plan view of sedimentary facies of any occurrence in a stratum. Since the stratigraphic interface that can be used for regional correlation is usually an unconformity surface, when we need to understand the sedimentary facies of the strata within a sequence we need to select a time interval above or below the unconformity surface for amplitude slicing. If the stratigraphic structure is parallel or subparallel, the horizon slices are cut along an isochronal plane, otherwise they may be cut along a diachronous surface. Therefore, for a set of strata with a diverging configuration, an isochronal interpretation of the top and bottom surfaces of the wedge is first required, then internal bisecting time interval slices can be made according to the top and bottom surfaces, i.e., stratal slicing (Zeng et al., 1998). The stratal slicing solves the problem of extracting the isochronal slice view of non-parallel strata without continuous internal reflections.

4.3.2.4. Ninety-degree phase shift. A 90° phase shifting transforms the minimum-phase wave into a zero-phase wave (Fig. 6). This makes thin interlayers correspond one to one to the strong phase, which reduces the phase number and improves the resolution of the thin interlayer reservoir (Zeng, 2018). But it also transforms a zero-phase wave into a minimum-phase wave, which confuses the corresponding relationship between event and stratigraphic interfaces (Brown, 2011) established by the zero-phase processing since the1970s. Generally, the 90° phase data is limited to research on thin bed reservoirs. The technique works well in deep-water deposits, where most sand bodies are less than a quarter of a wavelength thick and the lithofacies is dominated by mudstone and shale. And there have been some successful cases in other sedimentary environments in recent years.

4.3.2.5. Spectral decomposition. Spectral decomposition is a technique that breaks down seismic signals into narrow frequency sub-bands (Partyka et al., 1999). Such decomposition provides greater resolution

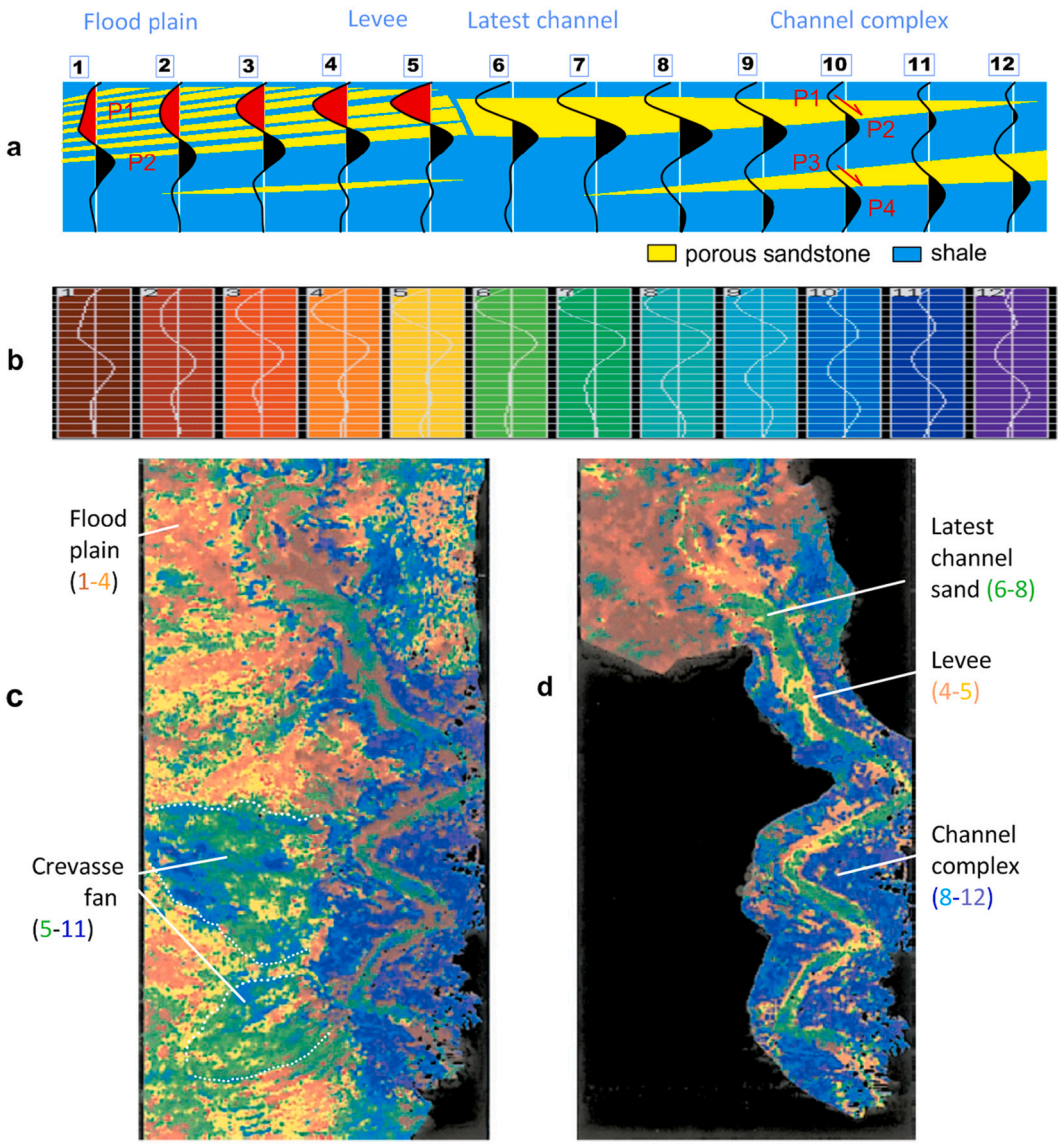

Fig. 27. Wave shape classifications of seismic facies, an example from south Texas, USA (modified from Brown, 2011; courtesy Flagship Geosciences LLC). a. Wave shape analysis: waveforms in 1–5, 6–10 and 11–12 traces indicate flood fan and levee, channel, and channel margin sandstone bodies, respectively; b. Wave shape classification of seismic traces over an interval of 100 ms; c and d. Seismic facies map showing a channel system where colors indicate the 12 different wave shapes classified in (b). (For interpretation of the references to colour in this figure legend, the reader is referred to the web version of this article.)

and detection of the layer-stacking heterogeneity, boundaries, and thickness variability than is possible with traditional broadband seismic attributes. Finding frequencies at which the geologic features stand out from the background amplitude is the key for the successful application of spectral decomposition to a dataset (Fig. 25) (Brown, 2011). This technique has been widely used to identify sandstone and shallow carbonate reservoirs of different thicknesses (Zeng et al., 2018; Yue et al., 2019).

The main purpose of spectral decomposition is to amplify the seismic reflection amplitude of sandstone bodies of different thickness by tuning, so that the sandstone bodies of different thickness can be clearly displayed in the seismic slice map. The basic working methods are as follows: first, high, middle and low frequency band wavelets are established by spectral decomposition; Secondly, three different seismic data volumes are synthesized from three wavelets and their common reflection coefficient data volumes, and the reflection amplitudes of thin, medium and thick sand bodies are amplified simultaneously; Third, three amplitude slice data are obtained from three seismic data volumes. Finally, the amplitude slice data of the three frequency bands are superimposed, so that the sand bodies of different thickness can be displayed with strong amplitudes.

Seismic profiles intercepted from high frequency band data volumes can improve the resolution of seismic waves (Miall, 2016). For example, according to the readable time thickness principle described above (section 2.4), the readable thickness of the sand body is 30 m in a conventional profile with a dominant frequency of 25 Hz, while it is 15 m in a seismic profile intercepted from the 52 Hz band data volume. Here the velocity of sandstone is 3000 m/s. However, because of the narrow frequency band, the side lobe energy of wavelets will be strengthened (Anstey, 1980), meaning many side lobe events without geological meaning will be added in these seismic sections, thus greatly weakening the correspondence between the event and geological interface. This is why high frequency band seismic profiles are not used for sequence stratigraphic research (Brown, 2011).

4.3.3. *Seismic geomorphology*

Although Brown et al. (1982) published the first seismic slice images showing meandering rivers back in the early 1980s, seismic

geomorphology was not widely studied until the late 20th century. Posamentier et al. (2007) defined seismic geomorphology as the application of analytical techniques pertaining to the study of landforms and to the analysis of ancient, buried geomorphical surfaces as imaged by 3D seismic data.

The seismic geomorphic image can be a single slice of seismic attributes or a slice of seismic attributes superimposed on the terrain, the latter was usually superimposed from current depth map and the attribute image of a given layer. If the paleogeomorphology is inconsistent with the present one, it can be reflected by the thickness of the stratum, but the relationship between the thickness of the stratum and the water depth needs to be clear (Xu et al., 2021). Seismic slice images extracted from shallow layers are usually slices of a surface or a horizon, which can display high-precision sedimentary landforms, and are mainly used in the study of Marine sedimentology, palaeoceanography, palaeoclimatology and mineral resources such as gas hydrates. In oil and gas exploration, the most commonly used attribute parameter is the root mean square amplitude, because it can better reflect the lateral changes of formation lithofacies in a time interval. With the help of 3D visualization and voxbody expression, the three-dimensional morphological characteristics of high-porosity sandstone and rivers can be displayed in suspension (Posamentier et al., 2007).

The seismic slice image map can be transformed into a sedimentary facies map through the comprehensive interpretation of seismic section and seismic slice images and drilling calibration. In general, in siliceous clastic formations with shale content greater than 15% and only two rock types: coarse-grained (including conglomerate, sandstone and siltstone) and fine-grained (including shale and mudstone), the lithology of the depositional elements can be determined using the commonly used six seismic parameters and slice images. Moreover, in such a simple lithofacies case, sandstone bodies can be delineated according to slice images, the depositional system is then reconstructed using the workflow of enhanced seismic lithofacies analysis. However, in the complex lithofacies environment, the use of slice images for the study of palaeogeomorphology and sedimentary facies is not recommended. This is because (1) different lithofacies bodies can show geometric images with similar characteristics. For example, extremely thick mouth bar sandstone, large set of flood mudstone and large set of volcanoclastic rock all show weak amplitude reflection or blank reflection; (2) Influenced by the superposition of the reflection wave of the strong reflection layer above or below the target layer, the slice image does not reflect the horizontal change of the lithofacies of the target layer, but the horizontal change of the overlying (or underlying) strong reflection layer, that is, the amplitude slice image reflects the palaeogeomorphology of the stratum above or below the target layer.

4.3.4. Seismic sedimentology

The concept of seismic topography was proposed by Zeng et al. (1998) and mainly refers to the high resolution fine description and sedimentological study of thin beds in 3d blocks. It is a school or branch of seismic facies analysis, rather than catchall for “all sedimentological research based on seismic data” as some Chinese scholars have defined.

Seismic sedimentology is supported by three key techniques: frequency decomposition, 90° phase shift, and formation sectioning. Spectral decomposition technology is mainly used to improve the resolution of thin bed; The 90° phase shift is used to reduce the number of seismic events in the formation of thin bed sandstone and shale, and to align the thin bed reservoir with seismic events (i.e., to the same depth). By using the stratal slicing technique, many isochronal slices can be made within a small range for continuous observation of vertical sedimentary environment and sedimentary facies changes. Using these techniques, the sedimentary environment, lithofacies and sedimentary processes in a region can be understood in greater detail (Fig. 26). Seismic sedimentology is mainly suitable for detailed description and sedimentological study of skeletal lithofacies bodies in a sedimentary body in simple lithofacies condition.

4.4. Auto-classification of seismic facies

Although seismic facies analysis is a comprehensive method combining seismic data and sedimentary geology, much of the process is beginning to be accomplished using artificial intelligence (AI). The software of wave shape classification (e.g., Salganicoff et al., 1988; Addy, 1998; Song et al., 2017) has been successfully applied to seismic facies analysis since the late 1990s (e.g., Addy, 1998; Coleou et al., 2003; Deng et al., 2008). The multi-attribute classification method is still at an experimental stage (e.g., Farzadi, 2006; Chopra and Marfurt, 2007; Saraswat and Sen, 2012; Amendola et al., 2017a; Di and Gao, 2017; Ross and Cole, 2017; Maurya and Singh, 2018; Verma et al., 2018; Zhao, 2018). Machine learning and data processing are new approaches that have emerged in recent years and are still in the early stages of exploration (e.g., Zhao et al., 2017; Wrona et al., 2018; Zhao, 2018; Ao et al., 2019).

4.4.1. Wave shape classification of seismic facies units

Wave shape classification uses neural network pattern recognition technology to classify the seismic facies units (Brown, 2011; Zahraa et al., 2017). Its basic working principles are as follows: the transverse variation of seismic reflection waveform is caused by the transverse variation of wave impedance structure; Each waveform is the seismic response of a stratum with a specific wave impedance structure; In a simple lithofacies environment, each wave impedance structure reflects a specific combination of rock types or a specific lithofacies; Similar waveforms reflect the same lithofacies (but may be of different sedimentary facies). The main working methods are as follows: (1) Based on well data and waveform analysis, the reflected waves of an isochronous stratigraphic unit are divided into N types of waveforms; (2) The neural network pattern recognition technology is used to automatically divide the reflected waveforms in a isochronous stratigraphic unit into N kinds of waveforms, and they are projected on the plan map to show the planar distribution of different waveforms. As each waveform or a set of waveforms can represent a seismic facies unit corresponding to a sedimentary facies unit, this kind of waveform classification map becomes a proxy for seismic facies distribution map.

There are many successful cases of wave shape classification, and one example provided by flagship Earth Sciences LLC is very representative (Fig. 27). In this example, seismic reflection waveforms within an isochronous unit in the study area are divided into 12 types (Fig. 27b), which represent lithofacies of 12 rock type combinations (Fig. 27a), and transverse changes in waveform and stratigraphic structure are continuous. The seismic reflection waves in this stratigraphic unit are then projected onto the planar view through 12 kinds of waveforms (the 12 waveforms on the plane are represented by 12 colors) to form a wave shape classification seismic facies plane image (Fig. 27c).

From the wave shape classification seismic facies map provided by the company, three seismic geomorphic units can be observed: narrow youngest channel, wide channel complex, crevasse fan and flood plain; five sedimentary elements can be identified: youngest channel sand, natural levee, channel complex, flood plain, and crevasse fan (or crevasse splay). The geological interpretation of the geomorphic units above is mainly based on the analysis of the genetic relationship between the waveform, acoustic impedance structure and sandstone layer structure: (1) The youngest channel sand body in mudstone is a relatively low-velocity interlayer, which generates the standard right downdip skew-symmetrical wave (RD wave) (waveforms 6 and 7, Fig. 27a); (2) There are two channel sand bodies in the channel complex, and two RD waves are generated (waveforms 8–12, Fig. 27a). The amplitude of a single RD wave varies with the thickness of its corresponding sand body; (3) A set of thin interbedded sandstones in the flood plain formation also produces RD wave (waveforms 1–4, Fig. 27a). However, because the vertical distribution width of thin interbedded sandstones is larger than that of single channel sand body, the waveform becomes wider and becomes low frequency wave. From waveform 5 to waveform 1, the

amplitude decreases due to the thinning of the accumulated thickness of the thin sandstone layers, and the wave shapes are similar due to their similar formation structure and wave impedance structure. (4) Similar to floodplain, natural levee also produces a low-frequency RD wave, whose amplitude is large due to the larger accumulated thickness (or porosity) of the thin sandstone layer (waveforms 4 and 5, Fig. 27a). (5) The plan geometry of crevasse fan is broad-leaved and has a variety of waveforms, including seismic reflection waveforms of the youngest channel and complex channels (waveforms 5–11, Fig. 27a), indicating that the stratigraphic structure of crevasse fans is the same as that of the complex channels.

The above example shows that the waveform classification technique is very effective for retrieving information about relatively low velocity reservoirs (porous sandstones and dolomites) and is a very good method, but due to the multiple solutions for the wave impedance structures of the lithofacies, it is also suitable for reservoir description of known sedimentary bodies.

4.4.2. *Multi-attribute classification of seismic facies*

The multi-attribute classification method uses amplitude, frequency, continuity, acoustic impedance, AVO, curvature, external form, internal structure, as well as some less commonly used parameters [such as music attribute (Amendola et al., 2017b) and speech recognition feature parameters (Xie et al., 2017)] to automatically classify seismic facies using the neural network pattern recognition technology (e.g., Meldahl et al., 2001; West et al., 2002; Coleou et al., 2003; Brown, 2011). There are many methods, including convolutional neural network, random forest, dictionary learning, k-means, and statistical clustering, multi-layer perceptron network, self-organizing mapping, support vector machine, terrain map generation, etc. (Zhao, 2018; Infante-Paez and Marfurt, 2019). The automation of seismic facies classification is a geophysicist's dream. They have worked hard for a long time, but so far the results have been less than ideal, which may be due to the following reasons: (1) Incomplete parameters. Regional seismic facies classification requires the use of all 9 independent parameters, as does a smaller block seismic facies analysis under complex geological conditions. Due to the lack of wave pattern, appearance, and other parameters, many key seismic facies cannot be distinguished at all, no matter what mathematical method is used. For example, without polarity or wave pattern parameters, it is impossible to distinguish whether the extra large amplitude reflection was generated by a low-velocity or a high-velocity interlayer. Similarly, it is impossible to distinguish whether a small amplitude reflection unit is produced by a set of sandstones or by a set of mudstones without using the parameter of appearance. (2) The effect of thickness (or spacing) on amplitude cannot be eliminated. (3) Many artificial intelligence researchers lack the background knowledge that combines seismic data and geology, which makes it difficult to translate the experience and knowledge of seismic interpreters into artificial intelligence processes.

Most importantly for AI methods, researchers need to fully understand the geological implications of the nine independent seismic parameters and to find the attribute parameters that replace these seismic markers. For example, Qi et al. (2016) were able to pick mass transported deposits by using the coherence and dissimilarity attributes. To a large extent, the two attributes used by them can replace the seismic parameter of reflection neatness or appearance of the seismic profile.

5. Summary

Seismic facies analysis is perhaps the most useful aspect of seismic stratigraphy, which emphasizes the integration of seismic data with geology. On a broader scale, it allows distinguishing sedimentary environments and interpreting lithologies based on seismic reflection geometry characteristics. Over the past several decades we have made great strides in rapidly extracting seismic information and displaying geologic bodies. Overall, however, the ability of researchers to extract geological information from seismic data is not yet extensive and needs to be improved by learning the basics of combined geophysics and geology, as well as more detailed "seicmic and geological dialogue" training. More detailed integration of seismic data and geology requires a procedure that involves: a) utilizing variations in velocity of different types of rocks with depth; b) wave impedance structure analysis with a thick layer (macroscopic layer) as the basic unit; c) matching analysis of the phase, wave pattern, and amplitude between synthetic seismograms and seismic records from a borehole; d) seismic simulation analysis of lateral variations in stratigraphic structure and rock type association; e) analyzing and inferring the geological properties of different wave shapes.

There are more than 100 parameters that can be used for seismic facies analysis, but there are only nine main independent parameters (i.e., spatial position, external form, internal configuration, continuity, smoothness, amplitude, frequency, neatness and wave pattern). In previous studies, most researchers used only a few of these parameters to analyze the sedimentary environment and lithofacies, which is feasible in simple sedimentary environment with only two rock types such as sandstone and shale, but not in complex geological conditions with multiple rock types. With the recent addition of three new parameters (neatness, smoothness, and waveform) researchers can now discriminate more detailed seismic lithofacies directly from seismic profiles, thereby greatly improving the accuracy of seismic facies analysis.

Traditional seismic facies analysis is based on seismic geometries that are similar to the geometries of a stratigraphic edifice or a sedimentary body, which can provide broader environment-of-deposition information. Seismic facies can be converted into sedimentary facies by ground-truthing through comparison with nearby borehole data, if available. The advantage of this working scheme is that it is easy to learn and employ. The disadvantage is that the identification accuracy for lithofacies away from the boreholes is weak, and the final result is often in the environmental sedimentary facies and lack of detailed lithofacies and hydrodynamic information. In the case of paucity of drilled holes and more complex geological conditions, the conversion of seismic facies to sedimentary facies lacks accuracy by traditional methods.

Enhanced seismic lithofacies analysis moves a step further than traditional lithofacies analysis by the use of additional parameters to identify lithofacies more accurately. It not only identifies more detailed seismic lithofacies directly from seismic profiles but can also generate information about flow paths through connecting midpoints of sedimentary domes and channels, the geometrical form of skeletal lithofacies, and about paleo-topography. Like in the traditional seismic facies analysis the major sedimentary environments can be established through shoreline, slope break, and foot of the slope mapping. A complete picture of the sedimentary system can be reconstructed by superposition of the environment, lithofacies, and flow path information. The advantage of this method is that it is not limited by data and can reconstruct a sedimentary system map with higher accuracy, which can be an upgrade version of the traditional seismic facies analysis.

Seismic slice image analysis can be used to study sedimentary systems by using slice view images and 3-D topography that is similar to the geometry of a sedimentary body. This method has an advantage of being able to describe the external morphology, internal structure, development, and distribution of the sedimentary body of interest in considerable detail. The disadvantage is that the application is the method is more effective in blocks where geological conditions are well understood and better-quality seismic reflection data is available. In areas with complex geological conditions and a paucity of drilling data the method is less effective. In addition, seismic sedimentological inferences based on frequency decomposition, 90°phase shift, and stratal slicing technology require specialized processing methods. Thus, seismic sedimentology is mainly suitable for the study of high-resolution seismic lithofacies (reservoir) of relatively smaller blocks where techniques developed for thin-bedded layers can find better utility.

The automatic classification method usually selects dynamic

attribute parameters and some geometric features and uses a mathematical approach to classifying seismic facies. The advantage of the wave shape classification method is that it is highly automated and can describe the sedimentary microfacies in detail. The disadvantage is that, in many cases, manual input may be required. It is also difficult to explain the geological properties of different waveforms without borehole calibrations. The multi-attribute classification method is still at an experimental stage, and to make this approach practical software engineers need to correctly apply the nine independent parameters discussed in this paper and incorporate real human expertise from experienced workers for deep machine learning.

In the future, the four work schemes of seismic facies analysis will not only undertake different tasks (Fig. 17), play different roles, but also learn from each other, infiltrate each other and develop together. Traditional seismic facies analysis is the common theoretical basis of the other three schemes. Enhanced seismic facies analysis proposed the "detailed lithofacies identification index system composed of nine independent parameters" and "a new path of sedimentary system reconstructed by the superposition of lithofacies, environment and flow path", which make up for the two short-comings of the traditional seismic facies analysis and improved the theoretical basis. Based on this enhanced theoretical basis, seismic facies analysis will usher in a new period of rapid development. Slice analysis and automatic classification schemes can explain the geological properties of slice and automatic classification plan view images more accurately; and more geological elements can be found in their seismic facies analysis results. The new detailed lithofacies identification index system will greatly improve the ability of lithofacies identification. This will not only improve the research level of basin sedimentology, but also help to improve the research level of other fields using seismic data, and will change the way of seismic profile observation. In the past, most researchers only observed reflection events, but in the future, not only reflection events (formation structure) will be observed, but waveform (lithofacies) will also be observed.

Declaration of Competing Interest

This manuscript has not been published or presented elsewhere in part or in entirety and is not under consideration by another journal. There are no conflicts of interest to declare.

Acknowledgements

We are indebted to Hengzhi Wu, Xiong Pang, Li Zhang, Dajun Peng, Lailiang Song, Die Hu, and Xue Xiao for their support of this research. We thank editors Christopher Fielding, Ian Candy and Andrew Miall, reviewer Dr. Zhuo Haiteng, and a number of other anonymous reviewers for their critical and constructive comments that have greatly improved the manuscript. We gratefully thank Guangzhou Marine Geological Survey, Southwest Petroleum Exploration and Development Research Institutes of PetroChina and SINOPEC, Research Institute of CNOOC for providing subsurface datasets, and for the permission to publish the results of this study. This research was jointly funded by National Major Science and Technology Projects of China (No. 2011ZX05025-003; 2016ZX05025-003), National Oil and Gas Resources Survey and Evaluation Strategic Projects of China (No. 2009GYXQ03-02; GZH201200511; DD0160155), first-class discipline construction plan of Chengdu University of Technology, and the Subsidy Scheme for Academic and Technical Leaders of Sichuan Province (No. 2009193).

References

Abbas, A., Zhu, H., Zeng, Z., Zhou, X., 2018. Sedimentary facies analysis using sequence stratigraphy and seismic sedimentology in the Paleogene Pinghu Formation, Xihu Depression, East China Sea Shelf Basin. Mar. Pet. Geol. 93, 287–297.
Addy, S.K., 1998. Neural network classification method helps seismic interval interpretation. Oil Gas J. 96 (37), 47–59.
Amendola, A., Gabbriellini, G., Dell'Aversana, P., Marini, A.J., 2017a. Seismic facies analysis through musical attributes. Geophys. Prospect. 65, 49–58.
Amendola, A., Gabbriellini, G., Dell'Aversana, P., Marini, A.J., 2017b. Seismic facies analysis through musical attributes. Geophys. Prospect. 65, 49–58.
Anstey, N.A., 1977. Seismic Interpretation: The Physical Aspects, 1977 edition. Springer, Boston. 625 pp.
Anstey, N.A., 1980. Seismic Exploration for Sandstone Reservoirs. IHRDC press, Boston, pp. 1–131.
Ao, Y., Li, H., Zhu, L., Ali, S., Yang, Z., 2019. Identifying channel sand-body from multiple seismic attributes with an improved random forest algorithm. J. Pet. Sci. Eng. 173, 781–792.
Badley, M.E., 1985. Practical Seismic Interpretation. IHRDC Press, Boston, pp. 1–259.
Barnes, A., 1994. Attributes for automating seismic facies analysis. In: 19. Seg Technical Program Expanded Abstracts, 2484 pp.
Batchelor, C.L., Dowdeswell, J.A., Pietras, J.T., 2013. Seismic stratigraphy, sedimentary architecture and palaeo-glaciology of the Mackenzie Trough: evidence for two Quaternary ice advances and limited fan development on the western Canadian Beaufort Sea margin. Quat. Sci. Rev. 65, 73–87.
Berg, O.R., 1982. Seismic detection and evolution of delta and turbidite sequence: their application to the exploration for the subtle trap. AAPG Mem. 32, 57–75.
Brown, A.R., 2011. Interpretation of three-dimensional seismic data. AAPG Mem. 42, 1–309.
Brown, A.R., Graebner, R.J., Dahm, C.G., 1982. Use of horizontal seismic sections to identify subtle traps. AAPG Mem. 32, 47–56.
Bubb, J.N., Hatlelid, W.G., 1977. Seismic stratigraphy and global changes of sea level, part 10: seismic recognition of carbonate buildups. AAPG Mem. 26, 185–205.
Caineng, Z., et al., 2011. Geological characteristics and forming conditions of the platform margin large reef-shoal gas province in the Sichuan Basin. Pet. Explor. Dev. 38 (6), 641–651.
Catuneanu, O., 2019. Model-independent sequence stratigraphy. Earth Sci. Rev. 188, 312–388.
Catuneanu, O., et al., 2009. Towards the standardization of sequence stratigraphy. Earth Sci. Rev. 92, 1–33.
Chen, L., Pang, X., Liu, J., Han, J.Y., Feng, X., 2015. Characteristics and identification of high quality deep-water gravity flow sandstone reservoirs in Baiyun sag, Pearl River Mouth Basin, South China Sea. Pet. Explor. Dev. 42, 507–515.
Chopra, S., Marfurt, K.J., 2007. Seismic Attributes for Prospect Identification and Reservoir Characterization (SEG geophysical developments series).
Chopra, S., Marfurt, K.J., 2012. Evolution of seismic interpretation during the last three decades. Lead. Edge 31 (9), 654–676.
Coleman, J.M., Wright, L.D., 1975. Modern river deltas: variability of processes and sand bodies. In: Broussard, M.L. (Ed.), Deltas, Models for Exploration. Houston Geological Society, Houston, pp. 99–149.
Coleou, T., Oupon, M., Azbel, K., 2003. Unsupervised seismic facies classification: a review and comparison of technique s and implementation. Lead. Edge 22 (10), 942–953.
Cukur, D., et al., 2012. Sedimentary evolution of Lake Van (Eastern Turkey) reconstructed from high-resolution seismic investigations. Int. J. Earth Sci. (Geol. Rundsch) 4, 1–15.
Davies, R.J., et al., 2004. 3D seismic technology: are we realising its full potential?. In: 3D Seismic Technology: Application to the Exploration of Sedimentary Basins, vol. 29. Geological Society, London, Memoir, pp. 1–9.
Deng, C., Yinji, J., Xiuhong, Z., 2008. Application of seismic waveform classification in predication of sedimentary microfacies(in Chinese wtih English abstract). Geophys. Prospect. Petrol. 47 (3), 262–265.
Di, H., Gao, D., 2017. Nonlinear gray-level co-occurrence matrix texture analysis for improved seismic facies interpretation. Interpretation 5 (3), 31–40.
Di, H., Alfarraj, M., AlRegib, G., 2018. Three-dimensional curvature analysis of seismic waveforms and its interpretational implications. Geophys. Prospect. https://doi.org/10.1111/1365-2478.12719.
Domenico, S.N., 1977. Elastic properties of unconsolidated porous sand reservoirs. Geophysics 42 (7), 1–7.
Farzadi, P., 2006. Seismic facies analysis based on 3D multi-attribute volume classification, dariyan formation, Se Persian Gulf. J. Pet. Geol. 29 (2), 159–174.
Fisher, W.L., McGowen, J.H., 1967. Depositional systems in the Wilcox Group of Texas and their relationship to occurrence of oil and gas. Gulf Coast Assoc. Geol. Socs. Trans. 105–125.
Galloway, W., Hobday, D.K., 1996. Depositional systems and facies within a sequence stratigraphic framework. In: Galloway, W.E., et al. (Eds.), Terrigenous Clastic Depositional Systems. Springer-Verlag Berlin Heidelberg, pp. 27–297.
Gong, C.L., et al., 2015. Shelf-edge trajectories and stratal stacking patterns: their sequence-stratigraphic significance and relation to styles of deep-water sedimentation and amount of deep-water sandstone. AAPG Bull. 99 (7), 1211–1243.
Gong, C.L., Steel, R.J., Wang, Y., Lin, C., Olariu, C., 2016. Shelf-margin architecture variability and its role in sediment-budget partitioning into deep-water areas. Earth Sci. Rev. 154, 72–101.
Guo, W., Xu, G.Q., Xu, S.H., Xu, Y.J., He, J.H., 2021. Influence of sediment supply rate on sequence stratigraphic architecture change: a case study from the Kaiping Sag, northern South China Sea. Mar. Pet. Geol. 129, 105106.
Gutiérrez-Paredes, H.C., Peterson-Rodríguez, R., Catuneanu, O., Hernández-Romano, U., 2018. Tectonic influence on the morphology, facies and distribution of Miocene reservoirs, southern Gulf of Mexico. J. S. Am. Earth Sci. 88, 399–414.
Haq, B., Hardenbol, J., Vail, P.R., 1987. Chronology of fluctuating sea levels since the triassic. Science 235, 1156–1167.
Hart, B.S., 2013. Whither seismic stratigraphy? Interpretation 1 (1), 3–20.

Horozal, S., et al., 2009. Seismic indicators of gas hydrate and associated gas in the Ulleung Basin, East Sea (Japan Sea) and implications of heat flows derived from depths of the bottom-simulating reflector. Mar. Geol. 258 (1–4), 126–138.
Hubbard, S.M., et al., 2011. Seismic geomorphology and sedimentology of a tidally influenced river deposit, lower cretaceous Athabasca oil sands, Alberta, Canada. AAPG Bull. 95, 1123–1145.
Infante-Paez, L., Marfurt, K.J., 2019. Using machine learning as an aid to seismic geomorphology, which attributes are the best input? Interpretation 7 (3), SE1–SE18.
Jiang, Zaixing, 2010. Sedimentology. Beijing, Petroleum Industry Press 1–424.
Kirk, R., 2016. Seismic Facies Mapping-Getting More Geology into Your Play. ASEG-PESA-AIG, pp. 1–8.
Klein, G.D., 1985. Sandstone Depositional Models for Exploration for Fossil Fuels. International Human Resources Development Corporation, Boston, Massachusetts, p. 209.
Koša, E., 2015. Sea-level changes, shoreline journeys, and the seismic stratigraphy of Central Luconia, Miocene-present, offshore Sarawak, NW Borneo. Mar. Pet. Geol. 59, 35–55.
Kumar, P.C., Omosanya, K.O., Sain, K., 2019. Sill Cube: an automated approach for the interpretation of magmatic sill complexes on seismic reflection data. Mar. Pet. Geol. 100, 60–84.
Leila, M., Moscariello, A., 2019. Seismic stratigraphy and sedimentary facies analysis of the pre- and syn- Messinain salinity crisis sequences, onshore Nile Delta, Egypt: Implications for reservoir quality prediction. Mar. Pet. Geol. 101, 303–321.
Li, H., Long, S., You, Y., Liu, G., Li, X., 2015. Sequence and sedimentary features of the Changxing Fm organic reefs and their control on reservoir development in the Yuanba Gas Field, Sichuan Basin (in Chinese with English abstract). Nat. Gas Ind. 2 (6), 506–514.
Liu, Z., 1997. Reservoir Seismic Stratigraphy (in Chinese with English Abstract). Geology Press, Baijing, pp. 1–257.
Liu, C., Xie, Q., Wang, G., Song, Y., Qi, K., 2016. Dolomite origin and its implication for porosity development of the carbonate gas reservoirs in the Upper Permian Changxing Formation of the eastern Sichuan Basin, Southwest China. J. Nat. Gas Sci. Eng. 35, 775–797.
Love, P.L., Simaan, M., 1984. Segmentation of stackes seismic data by the calssification of image texture. In: Expanded A bstracts of 54th Annual International SEG Meeting, pp. 536–537.
Luo, L.M., 1999. Three Dimensional High Resolution Sequence Stratigraphy of River and Lake Sedimentary Systems (in Chinese with English Abstract). Geological Press, Baijing, p. 187.
Ma, Y., Mou, C., Tan, Q., Yu, Q., Wang, R., 2007. Reef-bank features and their constraint to reservoirs of natural gas, from permian changxing formation to triassic feixianguan formation in Daxian-Xuanhan area of Sichuan Province, South China. Earth Sci. Front. 14 (1), 182–192.
Madon, M., Kim, C.L., Wong, R., 2015. The structure and stratigraphy of Deepwater Sarawak, Malaysia: Implications for tectonic evolution. J. Asian Earth Sci. 76, 312–333.
Majid, B., Mohammad, A.R., 2017. Modeling the facies of reservoir using seismic data with missing attributes by dissimilarity based classification. J. Earth Sci. 28 (4), 703–708.
Matenco, L.C., Haq, B.U., 2020. Multi-scale depositional successions in tectonic settings. Earth Sci. Rev. 200, 102991.
Maurya, S.P., Singh, N.P., 2018. Application of LP and ML sparse spike inversion with probabilistic neural network to classify reservoir facies distribution - a case study from the Blackfoot field, Canada. J. Appl. Geophys. 159, 511–521.
Meckel, L.D., Nath, A.K., 1977. Geologic considerations for stratigraphic modeling and interpretation. AAPG Mem. 26, 417–439.
Meldahl, P., Heggland, R., Bril, B., De Groot, P., 2001. Identifying fault and gas chimneys using multi-attributes and neural networks. Lead. Edge 20, 474–482.
Miall, A.D., 2016. Stratigraphy: A Modern Synthesis. Springer International Publishing Switzerland, pp. 1–442.
Mitchum, R.M., Vail, P.R., Sangree, J.B., 1977a. Seismic stratigraphy and global changes of sea level, part 6: stratigraphic interpretation of seismic reflection patterns in depositional sequences. AAPG Mem. 26, 117–135.
Mitchum, R.M., Vail, P.R., Thompson III, S., 1977b. Seismic stratigraphy and global changes of sea level, part 2: the depositional sequence as a basic unit for stratigraphic analysis. AAPG Mem. 26, 53–63.
Mitchum M, Robert, Van Wagoner C, John, 1991. High-frequency sequences and their stacking patterns: sequence-stratigraphic evidence of high-frequency eustatic cycles. Sedimentary Geology 70, 131–160.
Mutti, E., Normark, W.R., 1991. An integrated approach to the study of turbidite systems. In: Weimer, P., Link, M.H. (Eds.), Seismic Facies and Sedimentary Processes of Submarine Fans and Turbidite Systems. Springer-Verlag, New York, pp. 75–106.
Neidell, N.S., Poggiagliolmi, E., 1977. Stratigraphic modeling and interpretation-geophysical principles and techniques. AAPG Mem. 26, 389–417.
Nilsen, T., Shew, R., Steffens, G., Studlick, J., 2007. Atlas of deep-water outcrops. AAPG Bull. Stud. Geol. 56, 1–200.
Pacht, J.A., Bowen, B., Shaffer, L.B., 1993. Systems tracts, seismic facies, and attribute analysis within a sequence-stratigraphic framework—example from the Offshore Louisiana Gulf Coast. Mar. Clastic Reserv. 21–38.
Partyka, G.A., 2005. SEG Distinguished Lecture. http://eseg.org/staticcontent/presentations/partyka. Accessed September 15, 2009, SEG.
Partyka, G., Gridley, J., Lopez, J., 1999. Interpretational applications of spectral decomposition in reservoir characterization. Lead. Edge 18, 353–360.
Posamentier, H.W., 2000. Seismic stratigraphy into the next millennium. In: A Focus on 3D Seismic Data. American Association of Petroleum Geologists Annual Conference, New Orleans, LA, 16–19 April, 2000. A118.
Posamentier, H.W., 2001. Seismic geomorphology and depositional systems of deep water environments; observations from offshore Nigeria, Gulf of Mexico, and Indonesia (abs.). In: AAPG Annual Convention Program 10, 160 pp.
Posamentier, H.W., Allen, G., 1999. Siliciclastic sequence stratigraphy: concepts and applications. In: Concepts in Sedimentology and Paleontology, vol. 7. Society of Economic Paleontologists and Mineralogists (SEPM), p. 210.
Posamentier, H.W., Kolla, V., 2003. Seismic geomorphology and stratigraphy of depositional elements in deep-water settings. J. Sediment. Res. 73, 367–388.
Posamentier, H.W., Davies, R.J., Cartwright, J.A., Wood, L., 2007. Seismic geomorphology - an overview. Geol. Soc. Lond., Spec. Publ. 277, 1–14.
Prather, B.E., Booth, J.R., Steffens, G.S., Craig, P.A., 1998. Classification, lithologic calibration and stratigraphic succession of seismic facies from intraslope basins, deep. AAPG Bull. 82 (5A), 701–728.
Qi, J., Lin, T., Zhao, T., Li, F., Marfurt, K., 2016. Semisupervised multiattribute seismic facies analysis. Interpretation 4 (1), 91–106.
Rankey, E.C., 2017. Seismic architecture and seismic geomorphology of heterozoan carbonates: Eocene-Oligocene, Browse Basin, Northwest Shelf, Australia. Mar. Pet. Geol. 82, 424–443.
Ravenne, C., 2002. Sequence stratigraphy evolution since 1970. Comptes Rendus Palevol. 1 (6), 415–438.
Ricker, N., 1953. Wavelet contraction, Wavelet expression, and the control of seismic resolution. Geophysics 6 (18), 786–792.
Roksandic, M.M., 1978. Seismic facies analysis concepts. Geophys. Prospect. 26.
Ross, C.P., Cole, D.M., 2017. A comparison of popular neural network facies-classification schemes. Lead. Edge 36 (4), 340–349.
Roy, A., 2013. Latent Space Classification of Seismic Facies. University of Oklahoma.
Salganicoff, M., Sarna, M., Sax, L., Gerstein, G.L., 1988. Unsupervised waveform classification for multi-neuron recordings: a Leal-time, software-based system. I. Algorithms and implementation. J. Neurpsci. Meth. 25, 181–187.
Saller, A.H., Noah, J.T., Ruzuar, A.P., Schneider, R., 2004. Linked lowstand delta to basin-floor fan deposition, offshore Indonesia: an analog for deep-water reservoir systems. AAPG Bull. 88, 21–46.
Sangree, J.B., Widmier, J.M., 1977. Seismic stratigraphy and global changes of sea level, part 9- seismic interpretation of clastic depositional facies. AAPG Mem. 26, 165–185.
Saraswat, P., Sen, M.K., 2012. Artificial immune-based self-organizing maps for seismic-facies analysis. Geophysics 77 (4), 45–53.
Shanley, K.W., McCabe, P.J., 1994. Perspectives on the sequence stratigraphy of continental strata. Am. Assoc. Pet. Geol. Bull. 78, 544–568.
Sheriff, R.E., 1985. Aspects of seismic resolution. In: Berg, O.R., Woolverton, D.G. (Eds.), Seismic Stratigraphy II, AAPG Memoir, vol. 39, pp. 1–10.
Sheriff, R.E., Margaret, S.S., 1980. Seismic Stratigraphy. IHRDC Publishers.
Simm, R.W., White, R.E., 2002. Phase, polarity and the interpreter's wavelet. First Break 20, 277–281.
Song, C., Liu, Z., Wang, Y., Li, X., Hu, G., 2017. Multi-waveform classification for seismic facies analysis. Comput. Geosci. 101, 1–9.
Stow, D.A.V., Mayall, M., 2000. Deep-water sedimentary systems: new models for the 21st century. Mar. Pet. Geol. 17, 125–135.
Sun, Y., Wu, S., Dong, D., Lüdmann, T., Gong, Y., 2012. Gas hydrates associated with gas chimneys in fine-grained sediments of the northern South China Sea. Mar. Geol. 311-314, 32–40.
Vail, P.R., Mitchum, R.M., Thompson III, S., 1977. Seismic stratigraphy and global changes of sea level, part 3: relative changes of sea level from coastal onlap. AAPG Mem. 26, 63–83.
Vail, P.R., Audemard, F., Bowman, S.A., Eisner, P.N., Perez-Cruz, C., 1991. The stratigraphic signatures of tectonics, eustasy and sedimentology-an overview. In: Einsele, G., Ricken, W., Seilacher, A. (Eds.), Cycles and Events in Stratigraphy. Springer-Verlag, Berlin, pp. 617–659.
Verma, S., Bhattacharya, S., Lujan, B., Agrawal, D., Mallick, S., 2018. Delineation of early Jurassic aged sand dunes and paleo-wind direction in southwestern Wyoming using seismic attributes, inversion, and petrophysical modeling. J. Nat. Gas Sci. Eng. 60, 1–10.
Vermeer, G.J.O., 1998. Factors affecting spatial resolution. Lead. Edge 5 (17), 1025–1030.
Wang, Y.M., 1991. Seismic facies analysis, short course, lecture (3), Principle and Methods of Seismic Facies Analysis (in Chinese with English abstract). Sediment. Geol. Tethyan Geol. 4, 46–52.
Wang, H.Z., Shi, X.Y., 1998. Hierarchy of depositional sequences and eustatic cycles: a discussion on the mechanism of sedimentary cycles (in Chinese with English abstract). Geoscience 12 (01), 2–17.
Wang, Y., Liu, H., Xin, R., Jin, W.W.Y., Li, W., 2004. Lacustrine slope break: a new domain of strata and lithological trap exploration. Pet. Sci. 1 (2), 55–61.
Wang, C.C., Xu, G.Q., Zhuo, Y.H., 2015. Fundamental for Seismic-Geologic Interpretation (Chinese and English Edition). Petroleum Industry Press, Baijing, p. 126.
Wang, Y.Y., et al., 2019. A method for restoring sedimentary sequence original structural profiles: a case study of Miocene strata from the northern continental slope of the South China Sea. Mar. Pet. Geol. 88, 1–12.
Weidess, M.B., 1982. Quantifying resolution power of seismic systems. Geophysics 8 (47), 1160–1173.
West, P.B., May, R.S., Eastwood, E.J., Rossen, C., 2002. Interactive Seismic Facies Classification Using Textural Attributes and Neural Networks, vol. 21, pp. 1042–1049.
Widess, M.B., 1973. How thin is a thin bed? Geophysics 38 (6), 1176–1180.
Wrona, T., Pan, I., Gawthorpe, R.L., Fossen, H., 2018. Seismic facies analysis using machine learning. Geophysics 83 (5), 83–95.

Wu, H., Wu, Y., Ke, G., 2017a. Bioherm development model and reservoir prediction of Changxing Formation in Yuanba area,ortheastern Sichuan Basin (in Chinese with English abstract). Oil Gas Geol. 38 (4), 645–657.
Wu, Y., et al., 2017b. Fine prediction of reef boundary based on slope attributes: a case study of Permian Changxing Formation in Luodingzhai area, Sichuan Basin, SW China. Petrol. Explor. Dev. 44 (6), 960–971.
Xie, T., Zheng, X., Zhang, Y., 2017. Seismic facies analysis based on speech recognition feature parameters. Geophysics 82 (3), O23–O35.
Xu, G.Q., Pang, X., 2021. Sequence stratigraphic dynamics: Normal variation of the genetic stratigraphic unit driven by basin subsidence. Glob. Planet. Chang. 201, 103482.
Xu, H.D., Wang, S., Chen, K., 1990. Foundation of Seismic Stratigraphy Interpretation (in Chinese). China university of geosciences press, 182 pp.
Xu, G.Q., Li, G., Liu, S., 2005. Multiple karst cave horizons in the early Hercynian weathering crust in the Tarim basin (Chinese with English abstract). Acta Geol. Sin. 79 (4), 557–568.
Xu, G.Q., Pang, X., Ye, B., 2006. Discovering of turbidite fans in the Zhuhai formation in southern Baiyun sag and its significance, Pearl River Mouth Basin, China. In: Memoir of the 50th Anniversary of the Founding of Chengdu University of Technology, Chengdu:Sichuan Science Technology Publishing House, 192–195 (in Chinese with English abstract). Sichuan Science Technology Publishing House, Chengdu, pp. 192–195.
Xu, G.Q., Zhang, S.N., Li, Z.D., Song, L.L., Liu, H.M., 2007. Carbonate sequence stratigraphy of a back-arc basin: a case study of the QOM formation in the Kashan Area, Central Iran. Acta Geol. Sin. (Engl. Ed.) 81 (3), 488–500.
Xu, G.Q., et al., 2013. Stratigraphic division and depositional processes for the Mesozoic basin in Northern South China Sea. Mar. Geophys. Res. 34 (3), 175–194.
Xu, S.H., et al., 2015. Linking shelf delta to deep-marine deposition in reservoir dispersal of the upper Oligocene strata in the Baiyun Sag, the northern South China Sea. Aust. J. Earth Sci. 62 (3), 365–382.
Xu, S.H., et al., 2020. How much systems-tracts cale, three-dimensional stratigraphic variability is present in sequence stratigraphy?: an answer from the middle Miocene Pearl River Mouth Basin. AAPG Bull. 104, 1261–1285.
Xu, G.Q., et al., 2021. New method for the reconstruction of sedimentary systems including lithofacies, environments, and flow paths: a case study of the Xisha Trough Basin, South China Sea. Mar. Pet. Geol. 133, 105268.
Yue, D., et al., 2019. Fused spectral-decomposition seismic attributes and forward seismic modelling to predict sand bodies in meandering fluvial reservoirs. Mar. Pet. Geol. 99, 27–44.
Zahraa, A., Zailani, A., Ghosh, D.P., 2017. Characterizing geological facies using seismic waveform classification in Sarawak Basin. IOP Conf. Ser. 88, 1–21.
Zeng, H.L., 2011. Seismic sedimentology in China: a review (in Chinese with english abstract). Acta Sedimentol. Sin. 29 (3), 417–426.
Zeng, H., 2013. Frequency-dependent seismic-stratigraphic and facies interpretation. AAPG Bull. 97 (2), 201–221.
Zeng, H.L., 2018. What is seismic sedimentology? A tutorial. Interpretation 6 (2), 1–12.
Zeng, H.L., Henry, S.C., Riola, J.P., 1998. Stratal slicing, part II: real 3-D seismic data. Geophysics 63 (2), 514–522.
Zeng, H.L., et al., 2018. Carbonate seismic sedimentology: a case study of Cambrian Longwangmiao Formation, Gaoshiti-Moxi area, Sichuan Basin, China. Pet. Explor. Dev. 45 (5), 830–839.
Zhao, G., 2018. New horizons in geosciences: Application research of artificial intelligence in exploration geophysics in explosion. In: 2018 SEG Annual Conference Application Research Scan of Artificial Intelligence Technology in Exploration Geophysics, p. 23. Public number.
Zhao, T., Li, F., Marfurt, K.J., 2017. Constraining self-organizing map facies analysis with stratigraphy: an approach to increase the credibility in automatic seismic facies classification. Interpretation 5 (2), 63–71.
Zhou, L., et al., 2017. The seismic response characteristics and distribution of the reefs in the Changxing Formation, Northern Sichuan Basin (in Chinese with English abstract). Acta Petrol. Sin. 33 (04), 1189–1203.
Zhu, Xiaomin, 2003. Sequence Stratigraphy. Beijing, China University of Petroleum Press 1–207.
Zhu, Hongtao, et al., 2018. Varieties of sequence stratigraphic configurations in continental basins. Earth Sci. 43, 770–785.